Master Thesis

A Time-Frequency Localized Signal Basis for Multi-Carrier Communication

June 2010

Cornelis Willem Korevaar

Computer Architectures for Embedded Systems
Faculty of Electrical Engineering, Mathematics & Computer Science
University of Twente, The Netherlands

in cooperation with:
Ir. M.S. Oude Alink
Dr. Ir. A.B.J. Kokkeler
Prof. Dr. Ir. G.J.M. Smit

Abstract

The radio-spectrum has been untouched for centuries, but in recent years wireless devices have been competing more and more for some scarce bandwidth. As bandwidth auctions are billion-dollar affaires, wireless devices pop-up literally everywhere and forecasts state a 66x increase of data usage in just four years, an efficient use of the radio-spectrum is of ever increasing importance.

To arrive at a more efficient usage of the radio-spectrum, the presented work analyzes spectral leakage associated with Orthogonal Frequency Division Multiplexing (OFDM) and discusses solutions. Conventional solutions target the consequences, reducing sidelobes, rather than targeting the problems, the signals themselves. Instead, this thesis aims to arrive at a set of signals localized in time-frequency. The localization in time and frequency is lower-bounded by the uncertainty principle. The Hermite functions form a set of solutions to this lower-bound.

Although Hermite functions are optimally localized in time-frequency, that does not necessarily imply that the signals are also suitable for communication. Based on the discussion of ten signal attributes, criteria are formulated for a set of basis signals for communication. The Hermite functions are assessed based on these criteria and subsequently modified in order to meet the criteria. The resulting set of time-frequency localized signals, referred to as S_{TFL}, are in discrete-time, orthogonal, zero-mean, of equal energy and are localized in time and frequency.

Both OFDM and S_{TFL} signals asymptotically approach the optimum of 2 degrees of modulation freedom per time-bandwidth product. However, in case the spectrum becomes more and more utilized, mutual interference caused by conventional OFDM sidelobes severely degrades the effective data-throughput. Unlike OFDM, the signals S_{TFL} have a near-optimal localization and allow multiple users to communicate efficiently over time and frequency. The performance of S_{TFL} in mobile radio channels, the transceiver power efficiency and hardware complexity are discussed and compared to conventional OFDM, leading to minor differences between the two.

After all, given the increasing competition for some scarce bandwidth, there is good evidence to believe that the realization of transceivers employing Hermite functions, or their practical counterparts S_{TFL}, could be a major improvement in communication.

Preface

The world is changing: explosive demographic growth, merging cultures, urbanization, drastic environmental changes, increasing income inequalities, individualism, scarcity of numerous natural resources, loss of bio-diversity and the rise of global institutions are just a few of the many changes we recently experienced. The world has always been spinning around, but due to technological advances of last century, the momentum of changes seems to take new proportions. Despite the progress enabled by technology in fields like healthcare, production, logistics and telecommunications, many problems still exist along so many dimensions. It may be formulated as the ultimate goal of academia, and society as a whole, to find the solutions to the very problems today's world faces.

I have always been fascinated by problems. Whether it were mathematical, economical, business, engineering or the major challenges we are all confronted with. The university campus has facilitated me to work on a wide variety of topics related to mathematics and economics and their respective practices engineering and business. I came here to learn more about engineering and business in order to prepare to work in one of the fastest, most competitive sectors the business world knows: the consumer electronics market. During the years I have been hosted at the university, I am glad that I have been able to develop my engineering, business and entrepreneurial skills.

Some well-known scarce resources are water, food, energy and numerous raw materials. There is another, invisible scarce resource: the electromagnetic spectrum. It is used for conventional radio, cellular communication, satellite television, wireless internet and numerous other wireless communication applications. For each of these applications some bandwidth, part of the electromagnetic spectrum, is necessary for communication. As the number of wireless devices as well as their data usage is explosively growing, an efficient use of the electromagnetic spectrum is of increasing importance.

It may be familiar to you; you are tuning your FM radio to hear your favorite music station and you end up hearing noise and the cracky sound of other music stations. This is characteristic for wireless communication devices. Instead of using their own, isolated frequencies, wireless devices emit power over large parts of the spectrum causing interference to other devices. This issue, called spectral leakage, forms the primary topic of this thesis. A set of time-frequency localized signals for communication is proposed.

It was by my supervisors Mark Oude Alink, André Kokkeler and Gerard Smit that I got the classical and challenging problem of reducing spectral leakage. I am grateful for our fruitful discussions which I hope to continue in the near future. Above all, I would like to thank my parents, Hein & Reina Korevaar, for their support and the way they motivated me to do all the things I have done, so far...

Contents

1 Introduction 1

1.1 Wireless communications: an overview 1

1.2 Spectrum, a scarce resource 3

1.3 Problem definition & Research outline 4

1.4 Thesis Outline 5

2 Communication: A Time-Frequency Perspective 7

2.1 Time-frequency signal description 7

2.2 On sinusoidal multi-carrier modulation 8

2.3 Consequences of sinusoidal modulation 10

2.4 Overview of conventional solutions 12

2.5 On the extremes of time-limited and band-limited 13

2.6 Quest for a set of time-frequency optimal signals 15

3 A Time-Frequency Localized Signal Basis for Communication 19

3.1 Introduction 19

3.2 Hermite functions 19

3.3 The Dirac delta function investigated 22

3.4 Criteria on the basis set of signals 25

3.5 Assessment of the Hermite functions 29

3.6 Modification of the Hermite based signals 29

3.6.1 Discretization 29

3.6.2 Orthogonality & Uncorrelated 31

4 Performance Assessment 35

4.1 Performance measures 35

4.2 Transceiver & Simulation setup 35

4.3 Datarates 37

4.4 Multi-user application 40

4.5 Performance in mobile radio channels 42

4.5.1 Additive White Gaussian Noise channels 42

4.5.2 Fading channels 42

4.6 Peak to Average Power Ratio 45

4.7 Consequences for hardware 46

4.7.1 Transmitter 46

4.7.2 Receiver 47

4.8 Discussion of the results 47

5 Conclusions 49

5.1 Research aim & findings 49

5.2 Limitations & Discussion 50

5.3 Recommendations for future research 51

List of Acronyms 53

Bibliography 55

CHAPTER 1

Introduction

1.1 Wireless communications: an overview

The extensive use of the electromagnetic spectrum as a means to communicate started at the late 19th century. Wired communication already celebrated major milestones like the birth of the telegraph in the 1840s and the first transatlantic telegraph connection in 1858. Although it took an hour to transmit a few words [1], it has laid the basis for modern telecommunications. During the years that wired communication technology got started, Maxwell published his work *"A Dynamical Theory of the Electromagnetic Field"* in which he set out four well-known equations based on the work of Gauss, Ampère and Faraday [2]. Studying the electromagnetic field theory of Maxwell, Hertz and Tesla showed the principle of radio communication in a laboratory environment. It was M.G. Marconi who showed the world the use of radio waves by transmitting radio signals over the Atlantic Ocean around 1900. Although it would take decades for wireless communication to become mainstream, the first experiments of these early founders would pave the way for communication as we know it today.

In the 19th century wired communication was primarily used for the application of telegraphy. Communication was achieved by making and breaking an electric contact resulting in audible short pulses. When multiple users used the same line, users were scheduled after each other, which is nowadays known as Time Division Multiple Access (TDMA). One of the challenges of telegraph communication was to increase the user capacity of the lines. Bell examined the use of multiple frequencies to allow different telegraph users to communicate simultaneously. In 1876 he patented the idea of Frequency Division Multiplexing (FDM) [3]. In his patent, partly shown in figure 1.1, he describes a transmitter sending a sinusoidal wave giving a response by a telegraph machine tuned for that single frequency. By simultaneously sending several sinusoidal waves, each characterized by its own frequency, different telegraph connections are possible over a single line at the same time. Thanks to the invention of FDM the capacity of communication lines increased dramatically.

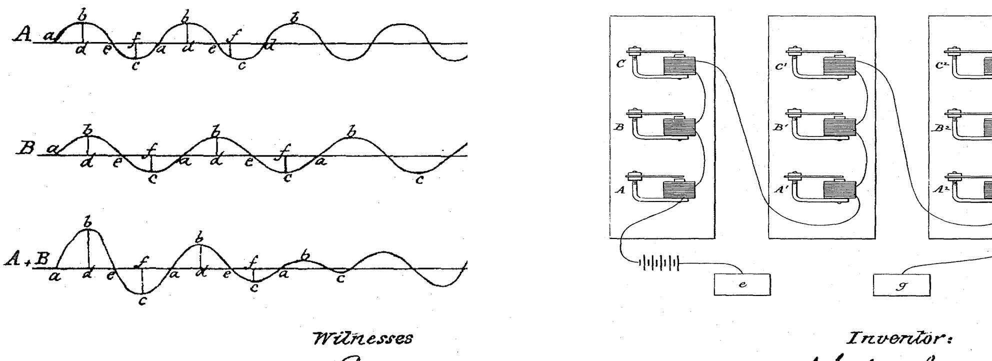

Figure 1.1 | Figures from U.S. patent no. 174.465, filed by A.G. Bell, explaining the ideas of Frequency Division Multiplexing [3]. Waves A and B of different frequency are summed to $A+B$ (left), sent over one single line, and excite a response in receiver A and receiver B tuned for waves of frequency A and B respectively (right).

In traditional FDM transmission systems, subchannels are placed apart in frequency with spectral guard space in between. Guard spaces are used to guarantee frequency isolation between different spectrum users. Although these guard bands prevent Inter-Carrier Interference (ICI), i.e. cross-talk between different carriers, the spectral efficiency is lowered as a result of non-information carrying guard spaces. A solution has been found by means of Orthogonal Frequency Division Multiplexing (OFDM). The orthogonality of the signals allow for a smaller subcarrier spacing. Thanks to the closer subcarrier spacing, communication using OFDM is possible at higher symbol rates than with traditional FDM. Important exploratory work has been performed by Chang & Gibby [4] and Saltzberg [5] in the 1960s who explored transmission systems using orthogonal waveforms. Full-cosine roll-off pulses, as shown in figure 1.2, were proposed by both authors. Note that the carrier spacing is now reduced from b for FDM to $b/2$ for OFDM. Saltzberg was the first who presented an OFDM-Offset Quadrature Amplitude Modulation (OQAM) transmission system, whereby both a sine and a cosine, which are orthogonal waveforms over $[0, 2\pi]$, are amplitude modulated. Despite their conceptual beauty, OFDM and the discussed OQAM variant had one important drawback: the computational complexity.

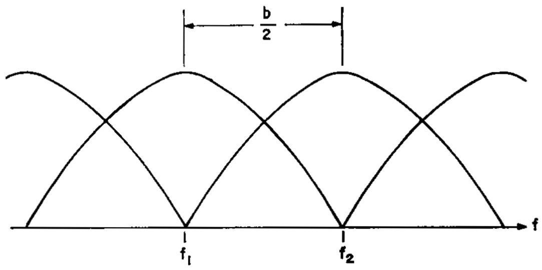

Figure 1.2 | Illustration of overlapping orthogonal (full cosine roll-off) pulses as proposed by Saltzberg in exploratory work on Orthogonal Frequency Division Multiplexing [5].

Cooley and Tuckey presented their fast implementation of the Discrete Fourier Transform (DFT) in 1965 [6]. It marked a major turning point in discrete signal processing, although it turned out that the algorithm itself was already found in a slightly different form by Gauss 150 years before [7]. However, the rediscovery of the Fast Fourier Transform (FFT) found its importance in various applications. For OFDM in particular the finding proved useful. The inverse and forward DFT were already suggested as a modulator and demodulator for OFDM to easily generate modulated sinusoidal waves of increasing frequency. A drawback was the computational complexity increasing quadratically with the number of carrier waves. This issue was addressed by Hirosaki who suggested the use of the inverse and forward FFT as modulator and demodulator for OFDM [8]. The computational complexity was now proportional to $N \log_2(N)$ compared to N^2 for the earlier DFT realizations.

The insight of using orthogonal signals together with the fast discrete Fourier implementations as modulator and demodulator would give OFDM a serious chance. Thanks to relatively small carrier bands, equalization reduces to a complex multiplication per subcarrier. The relatively long symbol times combat echoes associated with multi-path effects. Its ability to cope with multi-path effects has made OFDM especially popular for wireless applications. OFDM is used for Wireless Local Area Networks (WLANs), Digital Video Broadcasting - Terrestrial (DVB-T), Digital Audio Broadcasting (DAB) and many other wireless technologies.

1.2 Spectrum, a scarce resource

The electromagnetic spectrum is one of nature's scarce resources. Although large parts have been untouched for centuries, nowadays wireless devices are competing to get some some spectral bandwidth to enable communication. The frequencies useful for wireless communication range from about 30kHz to 300GHz, referred to as the radio-spectrum. European governmental institutions and the U.S. Federal Communications Commission (FCC) organize bandwidth auctions to provide telecommunications providers with bandwidth. An auction organized by the U.S. FCC in 2008 auctioned 52MHz bandwidth in the 700MHz range for 19.6 billion dollar [9]. The average price per MHz was about 400 million dollar. A report by Cisco Systems, presented by Morgan Stanley, forecasts a 66 times increase in mobile internet usage in four years [10]. This shall further intensify the battle for some scarce bandwidth.

Practically all wireless communication standards operate in fixed frequency bands and thereby occupy a part of the available spectrum. The supply of available channel capacity, dependent on Signal to Noise Ratios (SNRs) obtained in the channel as set out by the fundamental work of Shannon [11], is available independent of actual demand. A research carried out by the International Telecommunication Union (ITU) and the FCC shows that the use of radio spectrum, the part of the electromagnetic spectrum useful for radio communication, experiences large fluctuations [12]. For example, measurements carried out during the period from January 2004 to August 2005 show that frequency bands below 3GHz, on an average, have a utilization rate of 5.2% in the United States at any given location and time (for details refer to [13]). Similar conclusions can be drawn by looking at figure 1.3. We arrive at a paradox: on one hand spectrum is so scarce that telecommunication companies pay billions of dollars to obtain some bandwidth, while on the other hand the available link capacity is often not efficiently used. This paradox has been addressed by Mitola, who was the first to coin the concept of cognitive radio [14], whereby he advocates the use of intelligent, reconfigurable radios aware of their environment. We adopt the definition of cognitive radio as stated by the FCC [15]:

> *"A cognitive radio (CR) is a radio that can change its transmitter parameters based on interaction with the environment in which it operates. This interaction may involve active negotiation or communications with other spectrum users and/or passive sensing and decision making within the radio..."*.

Cognitive radios can employ Dynamic Spectrum Access (DSA) to come to a more efficient usage of the spectrum. DSA aims at real-time adjustment of spectrum utilization in response to changing circumstances and objectives [16]. Recently, much research has been devoted to the concept of cognitive radio. A standard for cognitive radio for Wireless Regional Area Networks (WRANs), the IEEE 802.22, is currently in development [17]. Also for Worldwide Interoperability for Microwave Access (WiMAX)

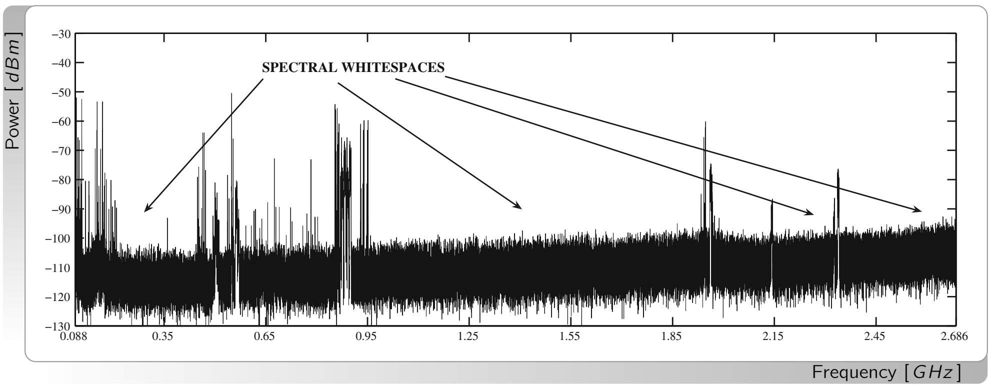

Figure 1.3 | Power Spectral Density from 88MHz to 2686MHz measured on July 11, 2008, in Worcester, MA [12]. Cognitive radios can sense the spectrum and dynamically set up connections to fill up the spectral whitespaces.

Cognitive radio dimension	Performance of OFDM/OFDMA as modulation technique
Spectral efficiency	Due to narrow-band subchannels, OFDM can effectively fill up the spectrum according to the channel conditions (the 'water-pouring principle') and establish communication close to the Shannon limit for the specified bandwidth. Nevertheless, a big challenge is the suppression of power leakage to adjacent channels in cognitive radio OFDM systems. Without limiting power leakage to adjacent channels, the overall spectral efficiency of an ensemble of unsynchronized OFDM-cognitive radios is severely degraded.
Channel robustness	Thanks to relatively large symbol times, OFDM is robust against multi-path effects. In addition, as a consequence of narrow-band subchannels, frequency selective fading affects only a few channels leading to a small degradation in BER. As OFDM depends on the orthogonality of signals in time and frequency, timing (jitter) and frequency errors lead to ISI and ICI respectively.
Adaptivity & Allocation	OFDM provides a number of flexible parameters like number of carriers, carrier power, frequency spacing and modulation which may vary over time, channel characteristics and user activity. Thanks to the FDM characteristic of OFDM, channels can easily be allocated to different active users [19].
Complexity	In general OFDM uses the inverse and forward FFT to efficiently implement the modulator and demodulator respectively. Thanks to narrow-band channels, equalization reduces to one complex multiplication per subcarrier. Analog challenges are caused by stringent phase noise requirements, a high Peak to Average Power Ratio (PAPR) and timing synchronization.
Inter-operability	With WLAN (IEEE 802.11), WMAN (IEEE 802.16), WPAN (IEEE 802.15.3a) and WRAN (IEEE 802.22) all using OFDM as their modulation technique, inter-operability between these standards is supported [19].

Table 1.1 | Cognitive radio dimensions and corresponding strengths and challenges concerning OFDM.

an amendment, IEEE 802.16h, is initiated as well as for WLANs, IEEE 802.11af, bringing cognitive radio elements into the standards. OFDM and in particular Orthogonal Frequency Division Multiple Access (OFDMA) are generally regarded as the primary candidates for cognitive radio [17], [18]. An overview of the strengths and challenges concerning the application of OFDM in cognitive radios is given in table 1.1.

1.3 Problem definition & Research outline

Due to an ever increasing number of wireless communication devices, one of nature's resources, the electromagnetic spectrum, is becoming increasingly scarce. The FCC chairman said in 2010: *"Our data shows there is a looming crisis. We may not run out of spectrum tomorrow or next month, but it is coming and we need to do something now"* [20]. In order to support this notice, regulatory bodies like the FCC allow wireless communication in licensed frequency bands under stringent criteria. For unlicensed operation in the U.S. television broadcast bands - among some other requirements - the following is specified: *"All unlicensed TV band devices will be required to limit their out-of-band emissions in the first adjacent channel to a level 55 dB below the power level in the channel they occupy, as measured in a 100 kHz bandwidth"* [21].

Cognitive radios employing DSA address the spectrum scarcity by dynamically setting up communication using spectrum whitespaces. In order to operate in the U.S. television bands, the cognitive radios should fulfill the requirement of 55dBc suppression of their out-of-band power. In order to meet this goal, the spectral leakage of cognitive radios should be drastically reduced. Two major sources of spectral leakage can be identified. First, OFDM is characterized by a sinc-shaped Power Spectral Density (PSD) whereby the OFDM sidelobes contain a significant amount of power. These sidelobes slowly decrease over frequency and can cause significant interference to other spectrum users. Second, non-linear components like filters and amplifiers cause intermodulation products. These may fall in-band, but also out-of-band, leading to undesirable interference to other devices. While the importance of reducing intermodulation products is acknowledged, this thesis primarily focuses on spectral leakage reduction related to OFDM.

From a spectrum scarcity perspective, the goal is to efficiently use the available spectrum over space and time. Efficient communication over space can be achieved by wireless devices using multiple antenna systems in combination with beam-steering and -forming. This research does not elaborate on the space dimension, but focuses on an efficient use of the radio spectrum over time and frequency. The aim is to reduce spectral leakage, while maximizing the effective data transfer rate and staying within energy, bandwidth and complexity budgets.

1.4 Thesis Outline

Chapter 2 addresses the problem of spectral leakage associated with OFDM. Solutions are discussed and an elaborate analysis leads to a set of Hermite functions as time- and frequency optimal signals. Chapter 3 starts with the formulation of criteria for a basis set of communication signals. The Hermite functions are assessed based on these criteria and subsequently modified in order to arrive at a set of time-frequency localized signals suitable for communication. Chapter 4 targets the performance of the proposed signal set under different circumstances and compare it to conventional OFDM. Finally, conclusions are drawn and recommendations are given for future work in chapter 5.

CHAPTER 2

Communication: A Time-Frequency Perspective

2.1 Time-frequency signal description

To get started, it may be useful to define some common signal properties. First a signal, as used in communication systems, may be described by its temporal and spectral behavior. The temporal and spectral behavior of the signals are linked by the Continuous Time Fourier Transform (CTFT) and its inverse:

$$F(\omega) = \int_{-\infty}^{\infty} f(t)\, e^{-j\omega t} dt \qquad f(t) = \frac{1}{2\pi} \int_{-\infty}^{\infty} F(\omega)\, e^{j\omega t} d\omega \tag{2.1}$$

where the normalization by $\frac{1}{2\pi}$ refers to the non-unitary transform. In upcoming sections, unless otherwise stated, these definitions are used as the forward and inverse Fourier transform. The unitary forward and inverse transforms are equal to equation 2.1 except for a (further) normalization by $\frac{1}{\sqrt{2\pi}}$ and $\sqrt{2\pi}$ respectively. The unitary Fourier transform is indicated by $\mathcal{F}_u$. There are a couple of practical limitations with the equations above. First, the transform assumes the signals to be defined on the whole time domain $[-\infty, \infty]$, while in practical communication systems signals often stretch over only one symbol limited in time. Second, as the concept of instantaneous frequency is not feasible, the spectrum $F(\omega)$ at time τ can only be found by localizing the function $f(t)$ around τ, giving rise to the Short Time Fourier Transform (STFT):

$$F_{st}(\tau, \omega) = \int_{-\infty}^{\infty} f(t) g(t-\tau)\, e^{-j\omega t} dt \tag{2.2}$$

While the integral of equation 2.2 still stretches from $-\infty$ till ∞ in time, a windowing function $g(t)$ has been introduced which is only nonzero for the region around $t = \tau$. In addition, the signals are in continuous time, while upcoming sections primarily deal with signals sampled in time. Assuming a sampling interval T, the signal $f(\tau, \omega)$ is only defined at the sampling points $n\Delta T$ whereby $n, m \in \mathbb{Z}$:

$$F_{st}(m, \omega) = \sum_{n=-\infty}^{\infty} f(n\Delta T) g\left((n-m)\Delta T\right)\; e^{-j\omega n\Delta T} \tag{2.3}$$

The equation above assumes the frequency description to be continuous, although in communication systems frequencies are often modulated and/or evaluated at specific frequencies $k\Delta F (k \in \mathbb{Z})$ only, i.e.:

$$F_{st}(m, k) = \sum_{n=-\infty}^{\infty} f(n\Delta T) g\left((n-m)\Delta T\right)\; e^{-j2\pi k\Delta F n\Delta T} \tag{2.4}$$

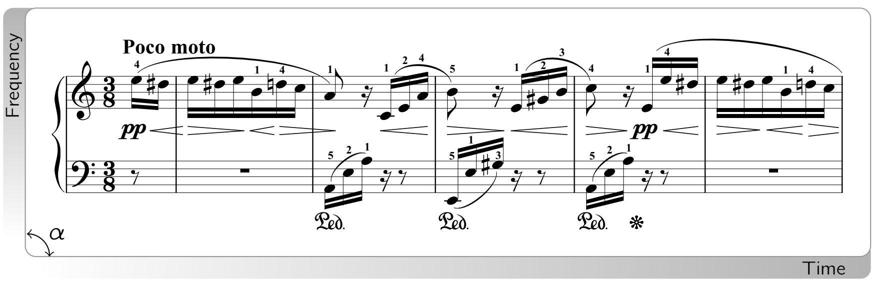

Figure 2.1 | Musical score as a metaphor to illustrate time-frequency interaction, i.e. signals varying over time (x-axis) and over frequency (y-axis). Opening notes of bagatelle no. 25, also known as *"Für Elise"* by Ludwig von Beethoven.

which describes the STFT of a time- and frequency-discrete signal $f(n\Delta T)$. Such a time- and frequency discrete signal representation can be illustrated with the metaphor of a musical score as shown in figure 2.1. The notes are played at distinct moments in time and represent tones of different frequencies. Although the equations prove to be useful in subsequent sections, it is important to bear in mind that true signals in analog transceivers are real continuous, time-varying signals.
As shown in figure 2.1, time and frequency are only two dimensions/extremes of the time-frequency lattice. The corner between the time- and frequency axis is indicated by α (and equals to $\pi/2$ in figure 2.1). Any intermediate time-frequency description can be obtained by means of the Fractional Fourier Transform (FrFT), which is in fact a generalization of the Fourier transform. The transform was proposed by Namias in relation to quantum mechanics [22] and later found application in optics. The FrFT corresponding to an angle $\alpha \in [-\pi, \pi]$ in the time-frequency plane is defined as [23]:

$$F_{u,a}(w) = \sqrt{\frac{1 - j\cot(\alpha)}{2\pi}} \cdot \int_{-\infty}^{\infty} f(t)\, e^{j\left(\frac{t^2}{2}+\frac{w^2}{2}\right)\frac{\cos(\alpha)}{\sin(\alpha)}} e^{-j\left(\frac{wt}{\sin(\alpha)}\right)} dt \tag{2.5}$$

For the special cases where α is $-\pi/2$ and $\pi/2$ the transform reduces to the forward and inverse unitary Fourier transform, respectively. The FrFT possesses many properties similar to the continuous time Fourier transform. For an overview of the FrFT related to signal processing, refer to the work of Almeida [23]. The FrFT proves to be useful for time-frequency analysis in upcoming sections.

2.2 On sinusoidal multi-carrier modulation

The main objective of communication may be described as transporting information from one person or node to another. In order to send information, some unique properties are necessary, which are understood by both transmitter and receiver. Radio-frequency communication is mostly based on harmonic radio waves. The frequency, phase and/or amplitude of the transmitted signals can contain information which are understood by the receiver. The corresponding domains stretch over $[0, \infty]$ for frequency, $[0, 2\pi]$ for phase and $[0, \infty]$ for amplitude. A sinusoidal signal varying over time as a function of amplitude A, phase ϕ and (radial) frequency ω can be described by:

$$f_{st}(A, \omega, \phi) = A \cdot \cos(\omega t + \phi) \tag{2.6}$$

The subscript $_{st}$ indicates that the function f as imposed by its parameters A,ϕ and ω, for any practical system, is limited in time and indicated as a short-time function. After some time a new signal, i.e. a new symbol, with information again encapsulated in A, ϕ and ω, is transmitted. The symbol time T_s represents the time-duration of a symbol. The transmitted signal may be described by the subsequent transmission of several symbols, i.e. sinusoids, multiplied by a weighting function $g(n)$ similar to the previously discussed STFT:

$$f(t) = \sum_{n=-\infty}^{\infty} f_{st}(A_n, \omega_n, \phi_n) \cdot g(t - nT_s) \tag{2.7}$$

whereby $g(n)$ is assumed equal for each symbol. The equation describes the transmit signal for a single carrier system as there is only one wave of frequency ω_n generated per symbol time. A multi-carrier transmission system deals with several carrier waves per symbol time, whereby each wave k is characterized by its own subcarrier frequency ω_k and may be modulated by a certain amplitude A_k and phase ϕ_k. The subcarrier waves can be summed and transmitted simultaneously, provided that the receiver is able to distinguish the different waves. A multi-carrier signal with K waves of different frequency, modulated by Amplitude Modulation (AM) and Phase Modulation (PM) using a sinusoidal base, can be described by:

$$f(t) = \sum_{n=-\infty}^{\infty} \sum_{k=0}^{K-1} A_{k,n} \cdot \cos(\omega_k \cdot t + \phi_{k,n}) \cdot g(t - nT_s) \tag{2.8}$$

The equation above does not specify what ω_k is. Ideally we would like to have the subcarriers closely spaced in frequency. The next exhibit discusses the minimum subcarrier spacing ΔF between ω_k and ω_{k+1} which is necessary to distinguish the different multi-carrier waves at the receiver.

◇ **Maximum number of sinusoidal subcarriers per time-bandwidth product**

In order to efficiently use the available bandwidth (given a certain time), the minimum frequency spacing ΔF needs to be calculated. Using a sinusoidal base, the frequency spacing is obtained by ensuring that the signals are mutually orthogonal [24]. The orthogonality condition over some symbol interval $[0, T_s]$ for two signals f_k and f_{k+1} is characterized by their frequencies ω_k and ω_{k+1}:

$$\int_{t=0}^{T_s} f_k\left(A_k, \omega_k, \phi_k\right) \cdot f_{k+1}\left(A_{k+1}, \omega_{k+1}, \phi_{k+1}\right) dt = 0 \tag{2.9}$$

Substituting equation 2.6, describing modulated sinusoids, the equality can be rewritten as:

$$A_k \cdot A_{k+1} \int_{t=0}^{T_s} \cos\left(\omega_k t + \phi_k\right) \cdot \cos\left(\omega_{k+1} t + \phi_{k+1}\right) dt = 0 \tag{2.10}$$

Using trigonometric identities and the substitution $\Delta\phi = \phi_{k+1} - \phi_k$ gives:

$$\frac{1}{2} \int_{t=0}^{T_s} \cos\left(\left(\omega_k - \omega_{k+1}\right) t - \Delta\phi\right) + \cos\left(\left(\omega_k + \omega_{k+1}\right) t + \Delta\phi\right) dt = 0 \tag{2.11}$$

Calculation of the integral over the symbol duration $[0, T_s]$ and subsequent simplification results in:

$$\begin{aligned} &\frac{1}{2} \sin\left(\Delta\phi\right) \left(\frac{\cos\left(\left(\omega_k - \omega_{k+1}\right) \cdot T_s\right) - 1}{\omega_k - \omega_{k+1}} - \frac{\cos\left(\left(\omega_k + \omega_{k+1}\right) \cdot T_s\right) - 1}{\omega_k + \omega_{k+1}} \right) \\ &+ \frac{1}{2} \cos\left(\Delta\phi\right) \left(\frac{\sin\left(\left(\omega_k - \omega_{k+1}\right) \cdot T_s\right)}{\omega_k - \omega_{k+1}} + \frac{\sin\left(\left(\omega_k + \omega_{k+1}\right) \cdot T_s\right)}{\omega_k + \omega_{k+1}} \right) = 0 \end{aligned} \tag{2.12}$$

Using the assumption $\left(\omega_k + \omega_{k+1}\right) \gg 1$ [24], filtering the high frequency modulation-product, the conditions for minimum frequency spacing become:

$$\sin\left(\Delta\phi\right) \left(\frac{\cos\left(\left(\omega_k - \omega_{k+1}\right) \cdot T_s\right) - 1}{\omega_k - \omega_{k+1}} \right) = 0 \tag{2.13}$$

$$\cos\left(\Delta\phi\right) \left(\frac{\sin\left(\left(\omega_k - \omega_{k+1}\right) \cdot T_s\right)}{\omega_k - \omega_{k+1}} \right) = 0 \tag{2.14}$$

For arbitrary values of $\Delta\phi$ the term $\left(\omega_k - \omega_{k+1}\right)$ should equal $2\pi m / T_s$, $m \in \mathbb{Z}$ in order to vanish to zero, while the lower equality gives the constraint that $\left(\omega_k - \omega_{k+1}\right)$ equals $\pi m / T_s$. When the phase difference $\Delta\phi$ is zero, the upper term vanishes, giving for the minimum frequency spacing $\Delta F = m / \left(2 T_s\right)$. For an unknown phase difference, e.g. in case of phase-modulation, the frequency spacing ΔF should be m / T_s in order to deal with orthogonal waveforms, i.e.:

$$\Delta F = \frac{\left|\omega_k - \omega_{k+1}\right|}{2\pi} = \begin{cases} m / \left(2 T_s\right) & \Delta\phi = 0 \\ m / T_s & \Delta\phi \in [0, 2\pi] \end{cases} \tag{2.15}$$

Concisely, the number of orthogonal sinusoidal waveforms K per time-bandwidth product is $2 \cdot BW \cdot T_s$ with BW the bandwidth and T_s the symbol duration. When both phase and amplitude modulation are used (for example in OFDM-(O)QAM), the phase difference $\Delta\phi$ for two sinusoidal waves can be any value, giving a minimum frequency spacing of $1/T_s$. These facts are graphically illustrated by figure 3.1. The left figure represents OFDM with amplitude and phase modulation while the right figure only allows for amplitude modulation. The number of degrees of freedom useful for modulation equal 2 per time-bandwidth product, which is the upper limit known from the fundamental work of Shannon [11].

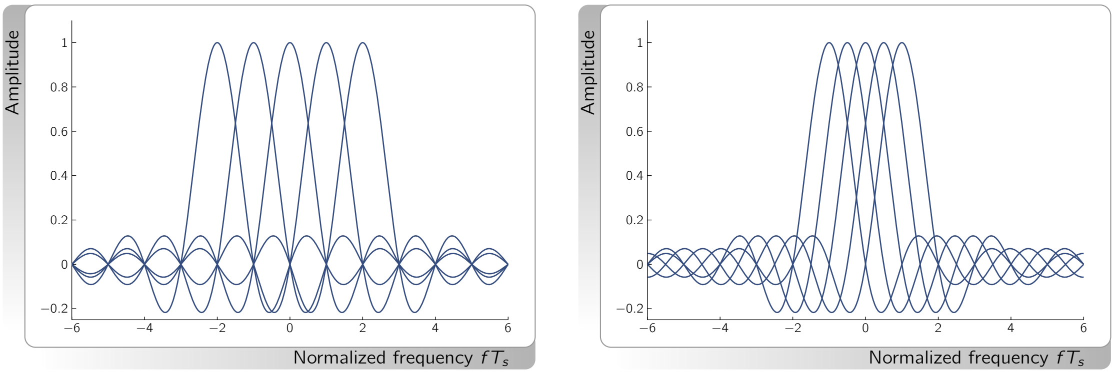

Figure 2.2 | Frequency presentation illustrating subcarrier spacing for five orthogonal sinusoids. Subcarrier spacing ΔF equals m/T_s for combined amplitude & phase modulation (left) and $m/2T_s$, $m \in \mathbb{Z}$ for amplitude modulation only (right).

2.3 Consequences of sinusoidal modulation

The previous section discussed the number of orthogonal sinusoidal waves fitting in a certain time-bandwidth product. The sinusoidal signals, as used in for example OFDM, can be modulated by phase and amplitude modulation. To recall the equation for an AM and PM multi-carrier signal with symbol duration T_s and subcarrier spacing according to equation 2.15 is:

$$f(t) = \sum_{k=0}^{K-1} \sum_{n=-\infty}^{\infty} A_{k,n} \cdot \cos\left(\frac{2\pi k}{T_s} \cdot t + \phi_{k,n}\right) \cdot g(t - nT_s) \tag{2.16}$$

Conventional communication systems extensively use the forward and inverse Fast Fourier Transform (FFT) to generate signals like equation 2.16. Due to the nature of the forward and inverse FFT the signals are windowed by a rectangular windowing function $g(t) = \text{rect}\,(t/T_s)$ over symbol time T_s. Using such a window the information, as represented by the sinusoidal phase and amplitude, can abruptly change from symbol to symbol. This leads to abrupt changes in the transmit signal as visualized by figure 2.3.

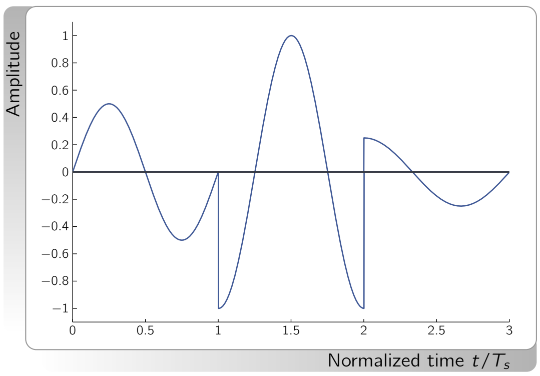

Figure 2.3 | Amplitude and phase modulated sinusoid for three consecutive symbol times (single carrier).

It may be apparent that the sharp, unnatural signal transitions shown in figure 2.3 give problems. The analog transceiver stages cannot deal with these sharp transitions (high frequency components) and the signals are likely to become distorted. Similarly, the time-limited signals cause spectral leakage which forms the topic of the next exhibit.

◇ **Wasting a scarce resource**
True sinusoids, as generated by the Fourier transform, are defined on the interval $[-\infty, \infty]$. In practice, the sinusoids as plotted in figure 2.3 only last for T_s seconds. The windowing function associated with the forward and inverse FFT is given by $g(t) = \text{rect}(t/T_s)$. For a single carrier, complex modulated signal at baseband the transmit signal can be described by:

$$f_k(t) = \sum_{n=-\infty}^{\infty} A_{k,n} \cdot e^{(j(2\pi k \Delta F t + \phi_{k,n}))} \cdot \text{rect}((t - nT_s)/T_s) \tag{2.17}$$

The equation describes the summation of an infinite number of time-limited complex exponentials with a certain amplitude and phase. To get a spectrum estimate we use the standard continuous Fourier Transform of equation 2.1, the superposition principle and the Fourier property of modulation giving the frequency representation:

$$F_k(\omega) = \sum_{n=-\infty}^{\infty} \frac{A_k}{2\pi} \cdot \mathcal{F}\left(e^{(j(2\pi k \Delta F t + \phi_{k,n}))}\right) * \mathcal{F}\left(\text{rect}((t - nT_s)/T_s)\right) \tag{2.18}$$

where $*$ denotes a convolution. The expression can be evaluated knowing that $\mathcal{F}(e^{j\omega_0 t}) = 2\pi\delta(\omega - \omega_0)$, $\mathcal{F}(x(t - t_0)) = X(\omega)e^{j\omega t_0}$, $\mathcal{F}(\text{rect}(t/\tau)) = \tau \cdot \text{sinc}(\omega\tau/(2\pi))$ and the Fourier property that a convolution of signal with a (shifted) dirac-pulse gives the original (shifted) signal:

$$F_k(\omega) = \sum_{n=-\infty}^{\infty} A_k T_s \cdot \text{sinc}\left(\left(\omega/(2\pi) - k \cdot \Delta F\right) T_s\right) e^{j\phi_{k,n}} e^{j\omega n T_s} \tag{2.19}$$

For multi-carrier modulation, the frequency representation yields a summation of K frequency shifted sinc-shaped functions, mathematically given by:

$$F(\omega) = \sum_{n=-\infty}^{\infty} \sum_{k=0}^{K-1} A_k T_s \cdot \text{sinc}\left(\left(f - k \cdot \Delta F\right) T_s\right) e^{j\phi_{k,n}} e^{j\omega n T_s} \tag{2.20}$$

Summarizing, phase and amplitude modulation with a rectangular windowing function causes a sinc-shaped PSD affecting more frequencies than only the specified bandwidth. The PSD for 5 adjacent subcarriers is plotted in figure 2.4. Even a guard space of 100 subcarriers (based on a single subcarrier PSD) is not enough to limit interference to other devices by 55dBc as required by the FCC [21]. That means that for multi-carrier systems based on conventional OFDM, spectral guard spaces of hundreds of subcarriers should be used in order to reduce the interference to acceptable levels.

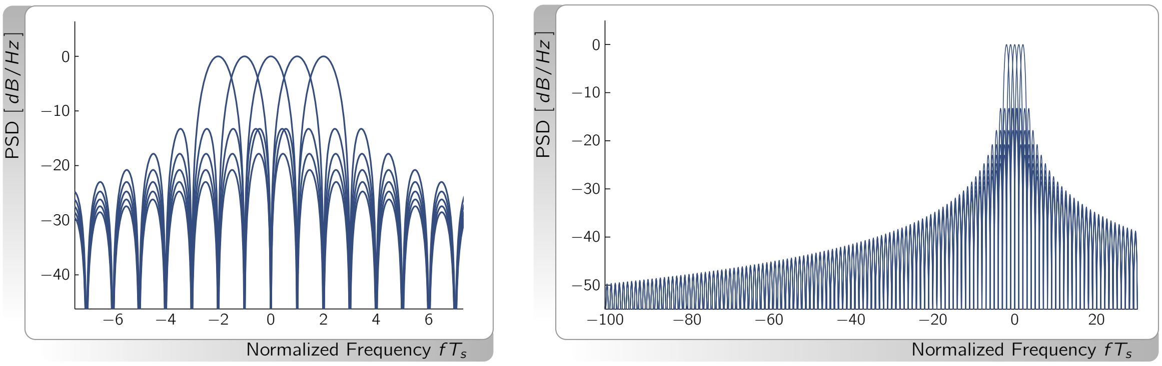

Figure 2.4 | PSDs of five adjacent OFDM subcarriers. Notice the slow decay of the sinc-shaped power spectra (right).

2.4 Overview of conventional solutions

The problem of OFDM sidelobes as encountered in the previous section has been faced by many scientists and engineers. This section discusses six general solutions to deal with the problem: *1. Guard spaces*, *2. Active Interference Cancellation (AIC)*, *3. Cancellation Carrier (CC)*, *4. Carrier weighting*, *5. Constellation mapping* and finally *6. Time-domain pulse-shaping*.

First, the traditional solution to cope with the OFDM sidelobes is to use large spectral *guard spaces*. A guard space is some unused spectrum which allows for the OFDM sidelobes to decay to acceptable levels. Guard spaces are a simple method to ensure frequency isolation among spectral users. Second, a more advanced method is offered by *Active Interference Cancellation (AIC)*. Predistortion is added to the OFDM signals such that the inserted signals cancel the OFDM sidelobes. Notches of about 40dB are achieved in this research while notches of even 80dB AIC have been published by Wang e.a. [25]. A third method to suppress OFDM sidelobes is based on *Cancellation Carriers (CCs)*. Some subcarriers are not used to carry information, but are modulated such that the sidelobes of these subcarriers nullify the sidelobes of the active subcarriers. Although suppression of about 10dB is feasible [26], drawbacks are the computational complexity, a significant increase in transmit power (25% in case of [26]) and a limited notch width. In case wider notches are desired more CCs are necessary. Fourth, sidelobes can also be suppressed by *weighting individual carriers* [27]. The weights of the subcarriers are chosen such that the sidelobes of one subcarrier cancel another. The weights are limited to a certain range to make sure that the subcarrier power does not vary too much and the Bit Error Rate (BER) is not severely degraded. The reported sidelobe suppression is about 10dB [27] & [28]. Fifth, as sidelobes in OFDM are caused by abrupt constellation changes, smart mapping of data onto constellation points can give smoother transitions than the ones shown in figure 2.3. Such *constellation mappings* are proposed by [29] and [30] reporting suppressions of nearly 10dB.

Finally, most research has been dedicated to *time-domain pulse-shaping*. The abruptly changing sinusoids and corresponding sharp signal transitions as shown in figure 2.3 are smoothened by a pulse-shaping filter. Among the large family of pulse-shaping filters a distinction can be made among Nyquist and non-Nyquist filters. Nyquist filters are generally known to be optimal for Inter-Symbol Interference (ISI) free transmission. On the other hand filters with a response equal to the time-reversed, conjugate signal templates (matched filters) are optimal in Additive White Gaussian Noise (AWGN) channels. Filters can be realized by an array of smaller band-pass filters, whereby the ensemble is referred to as a filter bank. Oversampled filter banks have become more and more popular in recent years as they allow for more advanced pulse-shapes than the rectangular pulse-shape associated with conventional OFDM. Oversampled or more general multi-rate filter banks do not only require Finite Impulse Response (FIR) or Infinite Impulse Response (IIR) filtering, but also operations like interpolation and decimation. For multi-rate operations a P-path polyphase implementation proves useful: an L-tap filter can then be implemented by P parallel filters of L/P taps operating at a sample rate of only $1/P$ of the original sample rate. A good overview of filter banks and implementations is given by Vaidyanathan [31]. More recent publications discuss oversampled filter banks using raised-cosine prototype filters [32], orthogonalized Gaussian prototype filters [33] and prototype filters derived by solving an optimization problem [34]. Sidelobe suppression of way over 40dB are regularly reported, although they typically come at the expense of large filter delays, excess bandwidths and a substantial increase in complexity.

Working with these six methods, one is likely to find himself ending up with the trade-offs like the ones sketched in figure 2.5. Interdependencies exist among all dimensions to a smaller or larger extent. The relation between datarate, power, noise and bandwidth are clarified by the Shannon limit [11]. Measures to increase the spectral efficiency, by reducing the OFDM sidelobes, are likely to have a negative impact on either transmit power, datarate and/or noise (less robustness against AWGN, time- and/or frequency dispersion).

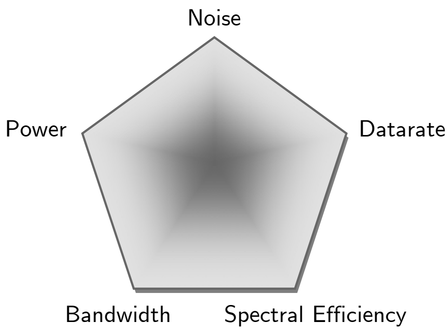

Figure 2.5 | Illustration of the trade-offs between power, datarate, noise, bandwidth and spectral efficiency. Measures to limit sidelobes, i.e. increasing the spectral efficiency, generally affect one of the other design dimensions.

It is important to notice that all methods discussed above do not change the basis signals themselves, but try to modify 'the-not-so-good' signals resulting from the inverse FFT modulator. It may be argued that the problems, i.e. the time-limited modulated Fourier signals, should be tackled at the root instead of dealing with the consequences. The Fourier transform and corresponding fast implementations have significantly advanced signal processing, although their convenience may have led to limited interest for other signal bases. Hence this research does not elaborate on the conventional solutions, but targets the basis signals used for communication. Upcoming sections deal with the quest for signals which are optimal from a time-frequency perspective.

2.5 On the extremes of time-limited and band-limited

Before diving into signal analysis, consider two extreme cases which are visualized in figure 2.6. On one hand, signals can be time-limited as is the case for conventional OFDM symbols. As discussed in section 2.3, large parts of the spectrum are polluted by the corresponding sinc-shaped power spectra. On the other hand signals can also be strictly band-limited, i.e. limited in frequency, while the signals spread over infinite time. As the time-presentation extends over infinite time, the signal is said to be non-causal. Both situations result in unnatural, unpractical signals with sharp transitions in time and frequency, respectively.

A question rises: what kind of signal is optimally localized in time-frequency? One of the theories underlying quantum mechanics is the uncertainty principle. The implications of the uncertainty principle can be split among three common dividers: first, the uncertainty principle relates characteristic features of quantum mechanical systems, second, it refers to ones inability to perform measurements on a system without changing it, and third and most interesting for us, it deals with harmonic analysis, *"A nonzero function and its Fourier transform cannot both be sharply localized"* [35]. The statement implies that a signal cannot be both time-limited and band-limited as its time and frequency behavior are related by the Fourier transform. This is in accordance with our observations in last section. The problem of suppressing out-of-band radiation while still aiming at datarates close to the Shannon limit can be reformulated to a new goal: finding signals that are optimally localized in time-frequency.

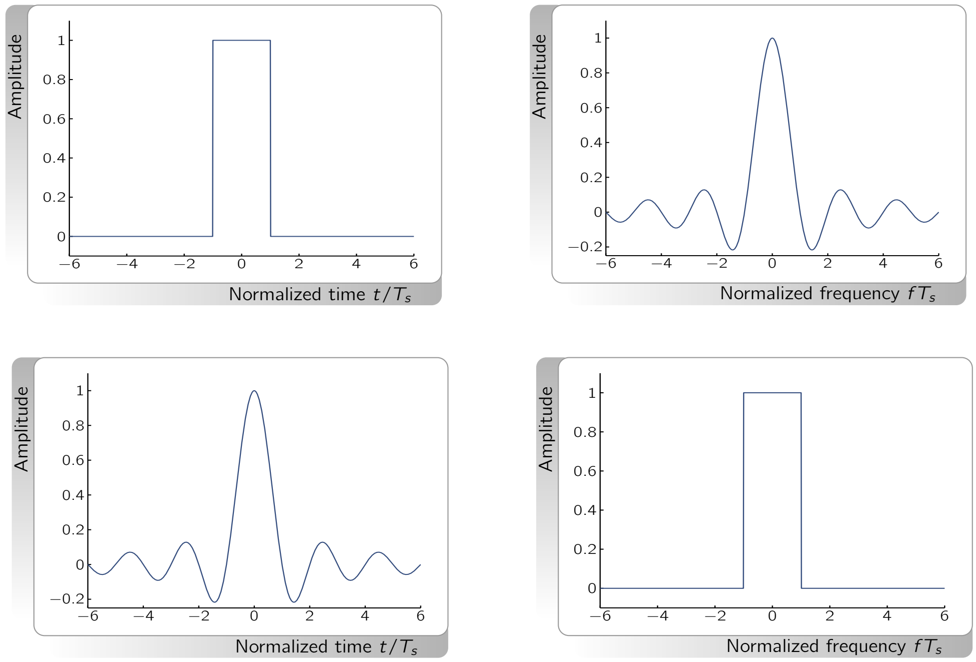

Figure 2.6 | The upper row of figures illustrates a time-limited signal with corresponding sinc-shaped frequency representation occupying theoretically infinite bandwidth. The other extreme, a band-limited signal, is illustrated by the lower row of figures. Note that the corresponding time-domain representation is non-causal.

◇ The uncertainty principle

Let us define a signal $f(t)$ and its Fourier transform $F(\omega)$ spanning the time-frequency plane. An expression for the localization of the energy of $f(t)$ in time is found by modeling the signal $f(t)$ as a stochastic process varying over time whereby the localization is found by the second order moment, its variance. In a similar way the localization of $F(\omega)$ in frequency can also be found. The variances in time and frequency are respectively:

$$\sigma_T^2 = \frac{\int_{-\infty}^{\infty} (t-t_0)^2 |f(t)|^2 dt}{\int_{-\infty}^{\infty} |f(t)|^2\, dt} \qquad \sigma_F^2 = \frac{\int_{-\infty}^{\infty} (\omega-\omega_0)^2 |F(\omega)|^2 d\omega}{\int_{-\infty}^{\infty} |F(\omega)|^2\, d\omega} \tag{2.21}$$

whereby the terms t_0 and ω_0 can be omitted when the moments around the origin are calculated. The general Heisenberg-Pauli-Weyl inequality, describing the uncertainty of a two-dimensional Hilbert space, indicates that the second order moments (variances) in time and frequency are lower bounded by the constraint:

$$\sqrt{\sigma_T^2 \cdot \sigma_F^2} \geq \frac{1}{2} \tag{2.22}$$

It is particularly interesting to find a function $f(t)$ which satisfies this equality. It is generally known that equality only occurs for the Gaussian function $f(t) = A \cdot e^{(-\alpha t^2)}$ on the domain $t = [-\infty, \infty]$ with Fourier transform $F(\omega)$ also being a Gaussian function $F(\omega) = A\sqrt{\pi/\alpha} \cdot e^{\left(-\frac{t^2}{4\alpha}\right)}$. When $\alpha = 1/2$, we have two Gaussian with equal variances satisfying the equality of equation 2.22. The equality is also met by other values of $\alpha \in \mathbb{R}$. Namely, scaling the function $f(t)$ in time by $f(\sqrt{\alpha}t)$ gives a frequency representation scaled by $(1/\sqrt{\alpha}) \cdot F(\omega/\sqrt{\alpha})$. The product of the variances, under different values of α, still equals the lower bound of equation 2.22:

$$\sqrt{\sigma_T^2 \cdot \sigma_F^2} = \sqrt{\left(\frac{1}{\sqrt{2}}\sqrt{\alpha}\right)^2 \cdot \left(\frac{1}{\sqrt{2}}\frac{1}{\sqrt{\alpha}}\right)^2} = \frac{1}{2} \tag{2.23}$$

We have arrived at a function: $f(t) = A \cdot e^{-\alpha t^2}$ with $F(\omega) = A\sqrt{\frac{\pi}{\alpha}} \cdot e^{\left(-\frac{t^2}{4\alpha}\right)}$ optimally localized in time-frequency. This in contrast with the sinc-shaped spectrum for conventional OFDM. Figure 2.7 shows a Gaussian pulse in a time-frequency plane.

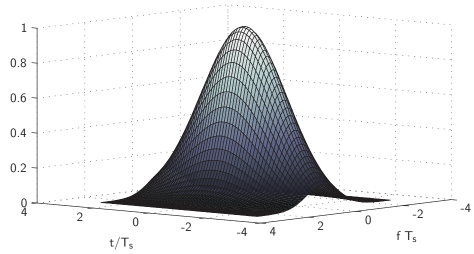

Figure 2.7 | Gaussian pulse in time-frequency lattice with minimal (but not necessarily equal) spread in time and frequency.

2.6 Quest for a set of time-frequency optimal signals

In section 2.6 the time-frequency optimization led to the Gaussian signal. But similar to the arguments leading to multi-carrier communication, we aim at a whole set of time-frequency localized signals, rather than a single signal. As equality in equation 2.22 is only achieved for the Gaussian signal, the constraint of an absolute minimum needs to be relaxed in order to find more solutions. The exhibit treats the quest for a set of time-frequency optimal solutions.

◇ **Solution set for time-frequency uncertainty**
Writing again the time-frequency uncertainty measure, as specified by equation 2.22, gives:

$$\sqrt{\sigma_T^2 \cdot \sigma_F^2} = \sqrt{\frac{\int_{-\infty}^{\infty} (t)^2 |f(t)|^2 dt}{\int_{-\infty}^{\infty} |f(t)|^2 \, dt} \cdot \frac{\int_{-\infty}^{\infty} (\omega)^2 |F(\omega)|^2 d\omega}{\int_{-\infty}^{\infty} |F(\omega)|^2 \, d\omega}} \tag{2.24}$$

The energy normalization performed by the denominators are linked by Parseval's identity, i.e. $\int_{\infty}^{\infty} |f(t)|^2 \, dt$ should equal $1/(2\pi) \int_{\infty}^{\infty} |F(\omega)|^2 \, d\omega$. Using Parseval's identity as well as the Fourier property $t^n f(t) \leftrightarrow (j)^n \frac{d^n}{d\omega^n} F(\omega)$, gives for the squared time-frequency uncertainty product:

$$\sigma_T^2 \cdot \sigma_F^2 = \frac{\frac{1}{2\pi} \int_{-\infty}^{\infty} \left| \frac{d}{d\omega} (F(\omega)) \right|^2 d\omega}{\frac{1}{2\pi} \int_{-\infty}^{\infty} |F(\omega)|^2 d\omega} \cdot \frac{\int_{-\infty}^{\infty} (\omega)^2 |F(\omega)|^2 d\omega}{\int_{-\infty}^{\infty} |F(\omega)|^2 d\omega} \tag{2.25}$$

Using the Cauchy-Schwarz inequality, a simplified expression can be found which is lower bounded by the uncertainty principle and upper bounded by equation 2.25, i.e.:

$$\frac{\frac{1}{2\pi} \int_{-\infty}^{\infty} \left| \frac{d}{d\omega} (F(\omega)) \right|^2 d\omega}{\frac{1}{2\pi} \int_{-\infty}^{\infty} |F(\omega)|^2 d\omega} \cdot \frac{\int_{-\infty}^{\infty} (\omega)^2 |F(\omega)|^2 d\omega}{\int_{-\infty}^{\infty} |F(\omega)|^2 d\omega} \geq \frac{\left(\int_{-\infty}^{\infty} \omega \cdot |F(\omega)| \cdot \left| \frac{dF(\omega)}{d\omega} \right| d\omega \right)^2}{\left(\int_{-\infty}^{\infty} |F(\omega)|^2 d\omega \right)^2} \geq \frac{1}{2} \tag{2.26}$$

The equality holds for Gaussian pulses as found in the previous exhibit. Now, relaxing the constraint of absolute equality, which is only valid for the Gaussian pulse, and restraining the signals to be normalized such that the denominators in equation 2.26 equal 1, the goal is to find a set of solutions minimizing the term $\left(\int_{-\infty}^{\infty} \omega \cdot |F(\omega)| \cdot \left| \frac{dF(\omega)}{d\omega} \right| d\omega \right)^2$. Note that we try to find $F(\omega)$; the corresponding time-domain representation is of course related by the Fourier transform. A comprehensive proof treated by Hilberg and Rothe [36] leads to the Weber equation:

$$\frac{d^2}{d\omega^2} F(\omega) - (\frac{1}{4}\omega^2 + \alpha) F(\omega) = 0 \tag{2.27}$$

Although [36] does not elaborate on the solutions of this equation, these are of particular interest for our quest of time-frequency optimality. When a solution $F(\alpha, \omega)$ exists for equation 2.27, then other solutions may also include $F(\alpha, -\omega)$, $F(-\alpha, j\omega)$ and $F(-\alpha, -j\omega)$ [37]. The differential equation has been the primary topic of a classical work by Whittaker [38]. He derived a set of standard solutions:

$$D_n(\omega) = \frac{j\Gamma(n+1)}{2\pi} e^{-\frac{1}{4}\omega^2} \omega^n \oint e^{-\lambda - \frac{1}{2}(\lambda^2/\omega^2)} \cdot (-\lambda)^{-n-1} d\lambda \quad \text{with } n = -\left(\frac{1}{2} + \alpha\right) \in \mathbb{N}_0 \tag{2.28}$$

whereby Γ is the gamma-function and path of integration is used as defined in [38]. This equation, in slightly modified form, has become generally known as the Whittaker function. Using Cauchy's n$^{\text{th}}$-order integration formula, the integral can (for $n \in \mathbb{N}_0$) be rewritten to [38]:

$$D_n(\omega) = (-i)^n e^{\frac{1}{4}\omega^2} \frac{d^n}{d\omega^n} \left(e^{-\frac{1}{2}\omega^2}\right) \quad \text{with } n = -\left(\frac{1}{2} + \alpha\right) \in \mathbb{N}_0 \tag{2.29}$$

These are exponentially weighted, probabilistic Hermite polynomials of degree n. As we dealt with four possible solutions, i.e. $F(\alpha, \omega)$, $F(\alpha, -\omega)$, $F(-\alpha, j\omega)$ and $F(-\alpha, -j\omega)$, substitutions in 2.29 give two sets of solutions:

$$D_n(\omega) = \begin{cases} e^{-\frac{1}{4}(\pm\omega)^2} He_n(\pm\omega) = e^{-\frac{1}{4}\omega^2} \left((-1)^n e^{\frac{1}{2}\omega^2} \dfrac{d^n}{d\omega^n} \left(e^{-\frac{1}{2}\omega^2}\right)\right) & \text{for } n = -\left(\frac{1}{2} + \alpha\right) \geq 0 \\ e^{\frac{1}{4}(\pm j\omega)^2} He_n(\pm j\omega) = e^{\frac{1}{4}\omega^2} \left(e^{-\frac{1}{2}\omega^2} \dfrac{d^{-n-1}}{d\omega^{-n-1}} \left(e^{\frac{1}{2}\omega^2}\right)\right) & \text{for } n = -\left(\frac{1}{2} + \alpha\right) < 0 \end{cases} \tag{2.30}$$

where $He_n(\omega) = (-1)^n e^{\frac{1}{2}\omega^2} \frac{d^n}{d\omega^n} \left(e^{-\frac{1}{2}\omega^2}\right)$ and $n \in \mathbb{Z}$. The second set of solutions corresponding to $F(-\alpha, \pm j\omega)$ gives solutions of unbounded energy as $\int_{\infty}^{\infty} D_n(\omega) d\omega \to \infty$ where $n > 0$. So we continue with the upper solution which is valid for $n \in \mathbb{N}_0$ and corresponding $\alpha = \{-\frac{1}{2}, -\frac{3}{2}, -\frac{5}{2}, ...\}$.

We may ask ourselves what the corresponding uncertainty product is. Therefore, we need to express the set of solutions corresponding to 2.27 in terms of their variances. We multiply equation 2.27 with $F^*(\omega)$, integrate over frequency $[-\infty, \infty]$ as suggested by [39] and finally apply integration by parts on the term $\frac{d^2}{d\omega^2} F(\omega)$, resulting in:

$$\frac{d}{d\omega} F(\omega) F^*(\omega) \Big]_{\infty}^{\infty} - \int_{-\infty}^{\infty} \frac{dF(\omega)}{d\omega} \frac{dF^*(\omega)}{d\omega} d\omega - \frac{1}{4} \int_{\infty}^{\infty} \omega^2 F(\omega) F^*(\omega) d\omega - \int_{\infty}^{\infty} \alpha F(\omega) F^*(\omega) d\omega = 0 \tag{2.31}$$

As we pursue frequency-localized, signals we may pose the condition that $F(\omega) = 0$ for $|\omega| \to \infty$. Thanks to this condition the first term cancels. The second term is exactly the description we found for σ_T^2, while the third term equals $\frac{1}{4}\sigma_F^2$ (using normalized 2.25). The fourth term equals α as the signal energy was normalized to 1. Altogether this results in:

$$\sigma_T^2 + \frac{1}{4}\sigma_F^2 = -\alpha \qquad \text{with } \alpha \in \{-\frac{1}{2}, -\frac{3}{2}, -\frac{5}{2}, ...\} \tag{2.32}$$

Equation 2.29 is known to be shape-invariant under the Fourier Transform. As the function is scaled in frequency by $\frac{\omega}{\sqrt{2}}$ the time-domain representation is scaled by $\sqrt{2}t$. Consequently, the frequency and time variances are scaled by 2 and $\frac{1}{2}$ respectively. This leads to $\sigma_F^2 = 4\sigma_T^2 \to \sigma_T^2 = -\frac{\alpha}{2}$ and thereby $\sigma_T^2 = (\frac{1}{4} + \frac{1}{2}n)$. Substituting $\sigma_T^2 = (\frac{1}{4} + \frac{1}{2}n)$ and $\sigma_F^2 = 4\sigma_T^2$ into 2.24 gives us the uncertainties for the time-frequency optimal solutions of equation 2.30 for $n \geq 0$:

$$\sqrt{\sigma_T^2 \cdot \sigma_F^2} = n + \frac{1}{2} \qquad \text{for } n \in \mathbb{N}_0 \tag{2.33}$$

The exhibit leads us to a set of time-frequency localized signals. These signals are time-frequency optimal in the sense of the Heisenberg-Pauli-Weyl uncertainty definition given by equation 2.22. The solutions found are known as Hermite functions and are weighted Hermite polynomials of degree n:

$$F(\omega) = e^{-\frac{1}{4}(\pm\omega)^2} He_n(\pm\omega) = e^{-\frac{1}{4}\omega^2} \left((-1)^n e^{\frac{1}{2}\omega^2} \frac{d^n}{d\omega^n} \left(e^{-\frac{1}{2}\omega^2} \right) \right) \tag{2.34}$$

The Hermite functions constitute the eigenfunctions of the Fourier transform and are equally shaped in time and frequency (discussed in chapter 3). Therefore the time-representations $f(t)$ are equal except for some normalization and a time/frequency scaling. Uncertainty products for the Hermite functions of degree n are:

$$\sqrt{\sigma_T^2 \cdot \sigma_F^2} = n + \frac{1}{2} \qquad \text{for } n \in \mathbb{N}_0 \tag{2.35}$$

The first Hermite function corresponds to the Gaussian pulse, which was already found in section 2.6. The Gaussian pulse has the minimum uncertainty product of an $\frac{1}{2}$. Every function of higher degree has a larger time-frequency uncertainty product in correspondence with equation 2.35. Treatments of uncertainty principles have been presented along other ways and are generally quite elaborate. A well-known treatment, along another way, is given by Hardy [40]. A more recent contribution discussing Hermite functions in relation to uncertainty can be found in [41].

This chapter led to a set of time-frequency localized signals, Hermite functions. Their properties as well as their suitability as a basis set of signals for communication form the primary topics of next chapter.

CHAPTER 3

A Time-Frequency Localized Signal Basis for Communication

3.1 Introduction

The time-frequency optimization in chapter 2 led to the Hermite functions as a set of optimal time-frequency localized communication signals. Although the Hermite functions are ideal from a time-frequency perspective this does not necessarily imply that the Hermite functions are also optimal for communication in the broader sense. This chapter first deals with a general overview of Hermite functions and their basic properties. Afterwards, a set of signal properties and criteria are formulated and the Hermite functions are assessed based on these criteria. Finally, the functions are adapted into a new set of signals such that all criteria are met to the best extent while preserving the time-frequency localization characteristic of Hermite functions. As stated in the problem definition, the ultimate goal is to find a signal set which has minimal spectral leakage, while maximizing the effective data transfer rate and staying within energy, bandwidth and complexity budgets.

3.2 Hermite functions

The Hermite functions appeared in chapter 2 to be a set of solutions to the Heissenberg-Pauli-Weyl uncertainty principle. This section dives into the definitions and properties of these Hermite functions.

The major building block of the Hermite function is the Hermite polynomial called after the French mathematician C. Hermite who investigated these polynomials. Despite the name, the first traces lead back to the work of Laplace [42]. The Hermite polynomials have two widespread definitions referred to as the probabilists' and physicists' definition. The probabilists' Hermite polynomials are sometimes confusingly referred to as the modified Hermite polynomials. The definition of the probabilists' and physicists' polynomials are respectively:

$$He_n(x) = (-1)^n \, e^{\frac{x^2}{2}} \frac{d^n}{dx^n} \left(e^{\frac{-x^2}{2}} \right) \qquad\qquad H_n(x) = (-1)^n \, e^{x^2} \frac{d^n}{dx^n} \left(e^{-x^2} \right) \tag{3.1}$$

with the notation adopted from Abramowitz and Stegun [37]. The relation between the probabilists' and physicists' variant is found by a substitution $x' = x/\sqrt{2}$ giving $He_n = 2^{-n/2} H_n(x/\sqrt{2})$. The six probabilists' and physicists' Hermite polynomials of lowest degree are respectively:

$$\begin{aligned}
He_0(x) &= 1 & H_0(x) &= 1 \\
He_1(x) &= x & H_1(x) &= 2x \\
He_2(x) &= x^2 - 1 & H_2(x) &= 4x^2 - 2 \\
He_3(x) &= x^3 - 3x & H_3(x) &= 8x^3 - 12x \\
He_4(x) &= x^4 - 6x^2 + 3 & H_4(x) &= 16x^4 - 48x^2 + 12 \\
He_5(x) &= x^5 - 10x^3 + 15x & H_5(x) &= 32x^5 - 160x^3 + 120x
\end{aligned} \tag{3.2}$$

We recognize the solution for time-frequency optimal signals, as given by equation 2.34, as a weighted version of the probabilists' Hermite polynomials. Therefore, unless otherwise stated, we restrict ourselves to the probabilists' version $He_n(x)$. The n^{th}-order differentiation of equation 3.1 involves for any polynomial degree n a term $P_n(x) \cdot e^{-x^2/2}$. Differentiation of this term gives according to the product-rule a term $P_n(x) \cdot -xe^{-x^2/2}$ and $\frac{d}{dx}\left(P_n(x)\right) \cdot e^{-x^2/2}$. Applying this to equation 3.1 gives a description for

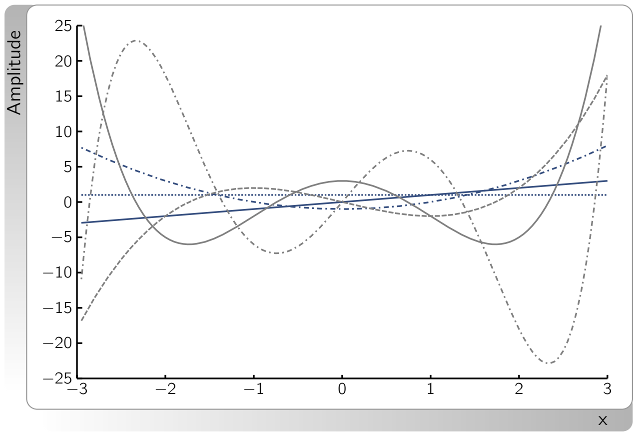

Figure 3.1 | The six probabilistic Hermite polynomials of lowest degree.

the polynomial sequence:

$$He_{n+1}(x) = xHe_n(x) - \frac{d}{dx}He_n(x) \tag{3.3}$$

The polynomial sequence satisfies $\frac{d}{dx}He_{n+1}(x) = n \cdot He_n(x)$ (see 3.2) and forms thereby an Appell sequence [42]. Substituting the equality, a recurrence relation can be deduced which is convenient for numerical calculation and digital implementation:

$$He_{n+1}(x) = x \cdot He_n(x) - n \cdot He_{n-1}(x) \tag{3.4}$$

The Hermite polynomials are part of the family of orthogonal polynomials. Other orthogonal polynomial sets include Chebyshev, Legendre and Jacobi polynomials. The Hermite polynomials of different degree are mutually orthogonal over the integration interval $[-\infty, \infty]$ with an exponential weighting function $g(x)$ [37]:

$$\int_{-\infty}^{\infty} He_n(x)He_m(x)g(x)dx = \begin{cases} 0 & \text{for } n \neq m \\ \sqrt{2\pi}n! & \text{for } n = m \end{cases} \qquad \text{for } g(x) = e^{-x^2/2} \tag{3.5}$$

If we split the weighting function into two parts and use $\sqrt{\sqrt{2\pi}n!}$ as a normalization (resulting from equation 3.5), we get two weighted orthonormal polynomials:

$$\int_{-\infty}^{\infty} \left(\frac{1}{\sqrt{\sqrt{2\pi}n!}} e^{-x^2/4} He_n(x) \right) \cdot \left(\frac{1}{\sqrt{\sqrt{2\pi}m!}} e^{-x^2/4} He_m(x) \right) dx = \begin{cases} 0 & \text{for } n \neq m \\ 1 & \text{for } n = m \end{cases} \tag{3.6}$$

We may refer to the first and second term as Hermite functions of degree n and m respectively. Hermite functions are usually associated with physicists' Hermite polynomials. To avoid further confusion, we refer to the functions based on probabilistic Hermite polynomials as *probabilistic Hermite functions* he_n. The functions $he_n(x)$ are built up by the Hermite polynomial He_n, the exponential weighting factor $e^{-x^2/4}$ and the normalization $1/\sqrt{\sqrt{2\pi}n!}$:

$$he_n(x) = \frac{1}{\sqrt{\sqrt{2\pi}n!}} e^{-x^2/4} He_n = \frac{1}{\sqrt{\sqrt{2\pi}n!}} e^{-x^2/4} \, (-1)^n \, e^{\frac{x^2}{2}} \, \frac{d^n}{dx^n} \left(e^{\frac{-x^2}{2}} \right) \qquad n \in \mathbb{N}_0 \tag{3.7}$$

The probabilistic (and physicist) Hermite functions possess an interesting property regarding their behavior in time and frequency. This property forms the topic of the exhibit. In subsequent sections the variable x is replaced by t when dealing with signals varying over time and by ω to represent radial frequencies.

◇ **Hermite functions: eigenfunctions of the (Fractional) Fourier Transform**

The Fourier transform is a powerful method for decomposing signals into a set of complex exponentials. As these exponentials are regarded as complex harmonic signals, the Fourier transform is said to transform signals to their frequency representation. Similar to other mathematical operators, there may exist signals which are invariant, not 'changing', under the Fourier transform. Such signals are the eigenfunctions of the operator and have corresponding eigenvalues.

It is generally known that the physicist Hermite functions constitute the eigenfunctions of the unitary CTFT. The physicist Hermite functions $h_n(t) = e^{-t^2/2} H_n(t)$ are shape-invariant under the transform, i.e.:

$$\mathcal{F}_u\left(h_n(t)\right) = \lambda h_n(t) \quad \text{with}\ \lambda = (-j)^n \tag{3.8}$$

This implies that the Fourier operator has an infinite number of eigenfunctions with four eigenvalues. The eigenvalues give a phase change of $n\pi/2$ and repeat over $4n$, which implies periodicity. The periodicity becomes more clear using the generalized FrFT. The fractional transform operation $\mathcal{F}_{u,\alpha}$ of the physicist Hermite functions is given in Namias fundamental work [22] and is given by:

$$\mathcal{F}_{u,\alpha}\left(h_n(t)\right) = \lambda h_n(t) \quad \text{with}\ \lambda = e^{-jn\alpha} \tag{3.9}$$

So any rotation in the time-frequency plane by an angle α leads to a shift in phase. As the degree of the polynomials increases, the phase changes faster. Instead of having real results only for $n = 4$ as for the CTFT, the FrFT yields a positive real eigenvalue of 1 for any $n\alpha = 2\pi$. This may be a useful property, although we do not further elaborate on this point. Note that for the case $\alpha = \pi/2$ the eigenvalues reduce to equation 3.8.

As the probabilistic Hermite functions are related to the physicists' Hermite functions by a scaling in time, $t' = t/\sqrt{2}$, and a normalization, the probabilists' Hermite functions are also equally shaped in time- and frequency, except for a scaling in time and frequency. We conclude with the unitary CTFT pair for the probabilistic Hermite functions:

$$he_n(t) \leftrightarrow (-j)^n 2 he_n(2\omega) \tag{3.10}$$

Summarizing, the Hermite functions are a special kind of signals which are not only optimally localized in time and frequency, but also have equally shaped time and frequency representations. The time and frequency representations of some probabilistic Hermite functions are given in figure 3.2. Notice that (for limited time-durations), the probabilistic Hermite functions of even degree have a non-zero mean, i.e. a DC component.

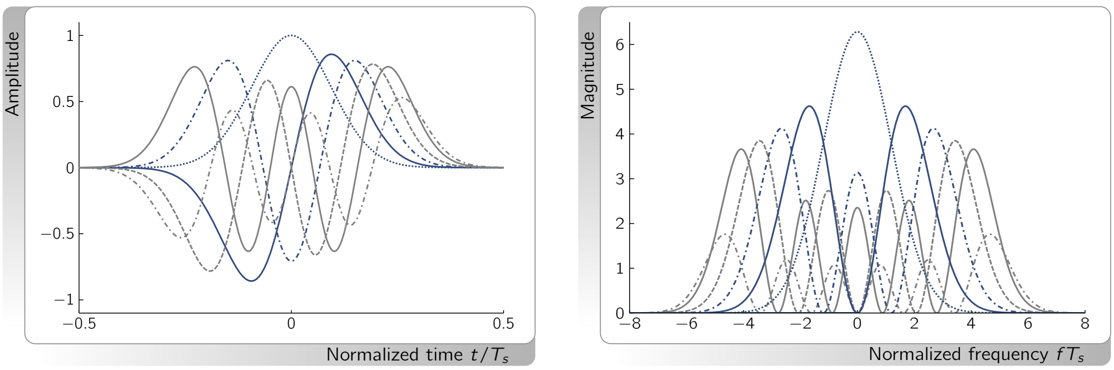

Figure 3.2 | The six probabilistic Hermite functions of lowest degree: time (left) and frequency (right) representations.

3.3 The Dirac delta function investigated

One of the most curious functions used in Fourier analysis is the Dirac delta function named after P.A.M. Dirac. Dirac himself called the function in 1926 an improper function [43]. This section discusses the Dirac delta function to learn more about its behavior, especially because it - according to Fourier theory - is closely related to the concept of frequency.

In order to analyze the delta function, we start using the property of the Hermite function as the eigenfunction of the Fourier operator. We split the physicist Hermite function of degree n into a normalization part $1/\sqrt{n!2^n\sqrt{\pi}}$, a polynomial and an exponential weighting factor. Although the physicist Hermite function h_n is used, the results are also applicable to the probabilistic Hermite functions he_n by an appropriate scaling in time and frequency. The physicist Hermite function is indicated by $h_n(t)$ and is given by:

$$\begin{aligned} h_n(t) =& \frac{1}{\sqrt{n!2^n\sqrt{\pi}}} e^{-t^2/2} H_n(t) = \frac{1}{\sqrt{n!2^n\sqrt{\pi}}} e^{-t^2/2} \left((-1)^n e^{t^2} \frac{d^n}{dt^n} \left(e^{-t^2} \right) \right) \\ =& \frac{1}{\sqrt{n!2^n\sqrt{\pi}}} \left(\alpha_n t^n + \alpha_{n-1} t^{n-1} + R_{n-2..0} \right) e^{-t^2/2} \end{aligned} \tag{3.11}$$

whereby the center term corresponds to the polynomial and $R_{n-2..0}$ comprises all lower order degree terms. We can rewrite the functions $h_n(t)$ in matrix form by using the coefficients as given by equation 3.2, which gives for the five physicist Hermite functions of lowest degree:

$$\begin{bmatrix} h_0(t) \\ h_1(t) \\ h_2(t) \\ h_3(t) \\ h_4(t) \\ \vdots \end{bmatrix} = \underbrace{\begin{bmatrix} \theta_0 & 0 & 0 & 0 & 0 & \cdots \\ 0 & \theta_1 & 0 & 0 & 0 & \cdots \\ 0 & 0 & \theta_2 & 0 & 0 & \cdots \\ 0 & 0 & 0 & \theta_3 & 0 & \cdots \\ 0 & 0 & 0 & 0 & \theta_4 & \cdots \\ \vdots & \vdots & \vdots & \vdots & \vdots & \ddots \end{bmatrix}}_{\Theta} \cdot \underbrace{\begin{bmatrix} 1 & 0 & 0 & 0 & 0 & \cdots \\ 0 & 2 & 0 & 0 & 0 & \cdots \\ -2 & 0 & 4 & 0 & 0 & \cdots \\ 0 & -12 & 0 & 8 & 0 & \cdots \\ 12 & 0 & -48 & 0 & 16 & \cdots \\ \vdots & \vdots & \vdots & \vdots & \vdots & \ddots \end{bmatrix}}_{A} \cdot \begin{bmatrix} t^0 \\ t^1 \\ t^2 \\ t^3 \\ t^4 \\ \vdots \end{bmatrix} \cdot e^{-t^2/2} \qquad \text{with } \theta_n = \frac{1}{\sqrt{n!2^n\sqrt{\pi}}} \tag{3.12}$$

As we are interested in the delta Dirac pulse, we apply the Fourier transform on the left and right sides of equation 3.11. We use hereby the Fourier property of modulation:

$$\mathcal{F}\left(h_n(t)\right) = \theta_n \cdot \frac{1}{2\pi} \left(\mathcal{F}\left(\alpha_n t^n + \alpha_{n-1} t^{n-1} + R_{n-2..0} \right) * \mathcal{F}\left(e^{-t^2/2} \right) \right) \tag{3.13}$$

In order to deal with the polynomial part, the Fourier property $t^n f(t) \leftrightarrow (j)^n \frac{d^n}{d\omega^n} F(\omega)$ can be used whereby $f(t) = 1$. We need to be careful with the transform of $f(t) = 1$. As the transform pair $1 \leftrightarrow 2\pi\delta(\omega)$ includes the function $\delta(\omega)$ of interest, we use a similar, but more complete statement $\lim\limits_{\beta\to\infty} f(t/\beta) = 1$. The corresponding Fourier transform becomes in the limit $\beta \to \infty$ equal to $2\pi\,|\beta|\,\delta(\beta\omega)$. Using this transform and working out the polynomial term of the convolution gives:

$$\mathcal{F}\left(\alpha_n t^n + \alpha_{n-1} t^{n-1} + R_{n-2..0} \right) = \lim_{\beta\to\infty} \beta \cdot 2\pi \left[\alpha_n (j)^n \frac{d^n}{dw^n} \delta(w) + \alpha_{n-1} (j)^{n-1} \frac{d^{n-1}}{dw^{n-1}} \delta(w) + \frac{\mathcal{F}\left(R_{n-2..0}\right)}{2\pi} \right]_{w=\beta\omega} \tag{3.14}$$

Substituting this equality as well as the Fourier transform for the Gaussian $\mathcal{F}(e^{-\alpha t^2}) = \sqrt{(\pi/\alpha)} e^{-\omega^2/4\alpha}$ gives for the Fourier transform of the Hermite function:

$$\mathcal{F}\left(h_n(t)\right) = \lim_{\beta\to\infty} \beta \cdot \theta_n \left[\alpha_n (j)^n \frac{d^n}{dw^n} \delta\left(w\right) + \alpha_{n-1} (j)^{n-1} \frac{d^{n-1}}{dw^{n-1}} \delta\left(w\right) + \frac{\mathcal{F}\left(R_{n-2..0}\right)}{2\pi} \right]_{w=\beta\omega} * \left(\sqrt{2\pi} e^{-\omega^2/2} \right) \tag{3.15}$$

Using the discussed property that the physicist Hermite function is the eigenfunction of the unitary Fourier operator $\mathcal{F}_u$ with eigenvalues $(-j)^n$ results in (compensating by $1/\sqrt{2\pi}$ for the non-unitary transform):

$$\sqrt{2\pi}(-j)^n h_n(\omega) = \lim_{\beta\to\infty} \beta \cdot \sqrt{2\pi}\theta_n \left[\alpha_n (j)^n \frac{d^n}{dw^n} \delta\left(w\right) + \alpha_{n-1} (j)^{n-1} \frac{d^{n-1}}{dw^{n-1}} \delta\left(w\right) + \mathcal{F}\left(R_{n-2..0}\right) \right]_{w=\beta\omega} * \left(e^{-\omega^2/2} \right) \qquad \text{with } \theta_n = \frac{1}{\sqrt{n!2^n\sqrt{\pi}}} \tag{3.16}$$

Calculation of the the first five Fourier transformed signals $h_n(\omega)$ by substitution of the coefficients of equation 3.12 gives:

$$\begin{bmatrix} (-j)^0 h_0(\omega) \\ (-j)^1 h_1(\omega) \\ (-j)^2 h_2(\omega) \\ (-j)^3 h_3(\omega) \\ (-j)^4 h_4(\omega) \\ \vdots \end{bmatrix} = \lim_{\beta\to\infty} \beta \cdot \Theta \cdot A \cdot \begin{bmatrix} (j)^0 & 0 & 0 & 0 & 0 & \cdots \\ 0 & (j)^1 & 0 & 0 & 0 & \cdots \\ 0 & 0 & (j)^2 & 0 & 0 & \cdots \\ 0 & 0 & 0 & (j)^3 & 0 & \cdots \\ 0 & 0 & 0 & 0 & (j)^4 & \cdots \\ \vdots & \vdots & \vdots & \vdots & \vdots & \ddots \end{bmatrix} \cdot \begin{bmatrix} \frac{d^0}{dw^0}\delta(w) \\ \frac{d^1}{dw^1}\delta(w) \\ \frac{d^2}{dw^2}\delta(w) \\ \frac{d^3}{dw^3}\delta(w) \\ \frac{d^4}{dw^4}\delta(w) \\ \vdots \end{bmatrix}_{w=\beta\omega} * e^{-\omega^2/2} \tag{3.17}$$

with Θ and A as given by equation 3.12. Now we can find our description for the function $\delta(\omega)$. The equality corresponding to the first row is given by:

$$\begin{aligned} (-j)^0 h_0(\omega) &= \lim_{\beta\to\infty} \beta (j)^0 \cdot (\theta_0 \cdot \delta(\beta\omega)) * e^{-\omega^2/2} \\ \frac{1}{\sqrt{\sqrt{\pi}}} e^{-\omega^2/2} &= \lim_{\beta\to\infty} \beta \cdot \left(\frac{1}{\sqrt{\sqrt{\pi}}} \cdot \delta(\beta\omega) \right) * e^{-\omega^2/2} \end{aligned} \tag{3.18}$$

It is generally known that the convolution of two Gaussian functions yields another Gaussian. Similarly the deconvolution of a Gaussian with another Gaussian again should give a Gaussian function. Two Gaussians with variances σ_1^2 and σ_2^2 result - by the operation of convolution - in a new Gaussian with variance $\sigma_1^2 + \sigma_2^2$. In order for equation 3.18 to hold, the function $\delta(\omega)$ could be a Gaussian function with a variance $\sigma^2 \to 0$ (which is in fact true thanks to the limit with β). The limit nonetheless seems to allow also other functions for $\delta(\omega)$ like $\sin(\omega)/\omega$. As a $\sin(\omega)/\omega$ convolved with a Gaussian does not lead to a new Gaussian function, the shape is not preserved unless the limit is applied. We elaborate on $\delta(\omega) = e^{-C\omega^2/2}$, whereby it is easily verified that $C \in \mathbb{R}$ can take any value (assuring that $C \ll \beta$). Nevertheless, we'll restrict to unit energy, as characteristic for the Dirac delta pulse, giving $C = 2\pi$.

◇ **Verification of higher order Hermite functions**

Now we have a description for $\delta(\omega)$, we should verify the validity of this notice for higher degree Hermite functions $h_n(\omega)$, $n > 0$. Therefore we first calculate the higher order derivatives of the delta function using the equality $\delta(\omega) = \frac{1}{\theta_0} h_0(\omega)$. We make use of the following general recurrence relation for Hermite functions [44]:

$$\frac{d}{d\omega} h_n(\omega) = \sqrt{\frac{n}{2}} h_{n-1}(\omega) - \sqrt{\frac{n+1}{2}} h_{n+1}(\omega) \text{ with } h_{-1}(\omega) = 0,\ h_0(\omega) = \frac{1}{\sqrt{\sqrt{\pi}}} e^{-\omega^2/2},\ n \in \mathbb{N}_0 \tag{3.19}$$

Using this recurrence relation, the higher order derivatives of the delta function $\delta(\omega)$ are:

$$\begin{bmatrix} \frac{d^0}{d\omega^0}\delta(\omega) \\ \frac{d^1}{d\omega^1}\delta(\omega) \\ \frac{d^2}{d\omega^2}\delta(\omega) \\ \frac{d^3}{d\omega^3}\delta(\omega) \\ \frac{d^4}{d\omega^4}\delta(\omega) \\ \vdots \end{bmatrix} = \frac{1}{\theta_0} \cdot \begin{bmatrix} 1 & 0 & 0 & 0 & 0 & \cdots \\ 0 & -\sqrt{\frac{1}{2}} & 0 & 0 & 0 & \cdots \\ -\frac{1}{2} & 0 & \sqrt{\frac{1}{2}} & 0 & 0 & \cdots \\ 0 & \sqrt{\frac{9}{8}} & 0 & -\sqrt{\frac{3}{4}} & 0 & \cdots \\ \sqrt{\frac{9}{16}} & 0 & -\sqrt{\frac{9}{2}} & 0 & \sqrt{\frac{3}{2}} & \cdots \\ \vdots & \vdots & \vdots & \vdots & \vdots & \ddots \end{bmatrix} \cdot \begin{bmatrix} h_0(\omega) \\ h_1(\omega) \\ h_2(\omega) \\ h_3(\omega) \\ h_4(\omega) \\ \vdots \end{bmatrix} \tag{3.20}$$

Substituting these descriptions of the higher order derivatives of $\delta(\omega)$ into equation 3.17 gives:

$$
\begin{bmatrix} (-j)^0 h_0(\omega) \\ (-j)^1 h_1(\omega) \\ (-j)^2 h_2(\omega) \\ (-j)^3 h_3(\omega) \\ (-j)^4 h_4(\omega) \\ \vdots \end{bmatrix}
= \lim_{\beta\to\infty} \beta
\underbrace{\begin{bmatrix} 1 & 0 & 0 & 0 & 0 & \cdots \\ 0 & \theta_1/\theta_0 & 0 & 0 & 0 & \cdots \\ 0 & 0 & \theta_2/\theta_0 & 0 & 0 & \cdots \\ 0 & 0 & 0 & \theta_3/\theta_0 & 0 & \cdots \\ 0 & 0 & 0 & 0 & \theta_4/\theta_0 & \cdots \\ \vdots & \vdots & \vdots & \vdots & \vdots & \ddots \end{bmatrix}}_{\Theta/\theta_0}
\cdot
\underbrace{\begin{bmatrix} 1 & 0 & 0 & 0 & 0 & \cdots \\ 0 & 2 & 0 & 0 & 0 & \cdots \\ -2 & 0 & 4 & 0 & 0 & \cdots \\ 0 & -12 & 0 & 8 & 0 & \cdots \\ 12 & 0 & -48 & 0 & 16 & \cdots \\ \vdots & \vdots & \vdots & \vdots & \vdots & \ddots \end{bmatrix}}_{A}
$$
$$
\cdot
\underbrace{\begin{bmatrix} (j)^0 & 0 & 0 & 0 & 0 & \cdots \\ 0 & (j)^1 & 0 & 0 & 0 & \cdots \\ 0 & 0 & (j)^2 & 0 & 0 & \cdots \\ 0 & 0 & 0 & (j)^3 & 0 & \cdots \\ 0 & 0 & 0 & 0 & (j)^4 & \cdots \\ \vdots & \vdots & \vdots & \vdots & \vdots & \ddots \end{bmatrix}}_{J}
\cdot
\underbrace{\begin{bmatrix} 1 & 0 & 0 & 0 & 0 & \cdots \\ 0 & -\sqrt{\frac{1}{2}} & 0 & 0 & 0 & \cdots \\ -\frac{1}{2} & 0 & \sqrt{\frac{1}{2}} & 0 & 0 & \cdots \\ 0 & \sqrt{\frac{9}{8}} & 0 & -\sqrt{\frac{3}{4}} & 0 & \cdots \\ \sqrt{\frac{9}{16}} & 0 & -\sqrt{\frac{9}{2}} & 0 & \sqrt{\frac{3}{2}} & \cdots \\ \vdots & \vdots & \vdots & \vdots & \vdots & \ddots \end{bmatrix}}_{D}
\cdot
\begin{bmatrix} h_0(w) \\ h_1(w) \\ h_2(w) \\ h_3(w) \\ h_4(w) \\ \vdots \end{bmatrix}_{w=\beta\omega}
* e^{-\omega^2/2}
\tag{3.21}
$$

Multiplication of the three matrices $\frac{1}{\theta_0}\Theta AJD$ involves quite a lot of multiplications, but gives a fairly simple result:

$$
\begin{bmatrix} (-j)^0 h_0(\omega) \\ (-j)^1 h_1(\omega) \\ (-j)^2 h_2(\omega) \\ (-j)^3 h_3(\omega) \\ (-j)^4 h_4(\omega) \\ \vdots \end{bmatrix}
= \lim_{\beta\to\infty} \beta
\begin{bmatrix} +(j)^0 h_0(\beta\omega) * e^{-\omega^2/2} \\ -(j)^1 h_1(\beta\omega) * e^{-\omega^2/2} \\ +(j)^2 h_2(\beta\omega) * e^{-\omega^2/2} \\ -(j)^3 h_3(\beta\omega) * e^{-\omega^2/2} \\ +(j)^4 h_4(\beta\omega) * e^{-\omega^2/2} \\ \vdots \end{bmatrix}
\tag{3.22}
$$

The left and right sides are equal in the limit where $\beta \to \infty$. So we have verified that $\delta(\omega) = e^{-\omega^2/\pi}$ not only holds for $n = 0$, but also for degrees up to 4. Similarly one should be able to proof validity for any n.

Summarizing, the Fourier transform of Hermite functions implies that the Dirac delta function involved equals a Gaussian function in order for the eigenfunction property of the Hermite functions to hold. The delta function suggested is described by:

$$
\delta(\omega) = \lim_{\beta\to\infty} \beta e^{-(\beta\omega)^2/\pi} \tag{3.23}
$$

Delta/impulse functions got primary interest of several mathematicians like Cauchy, Poisson and Hermite. We find good support in the delta function as proposed by Kirchhoff, who used it for the formulation of Huygens' principle in wave theory [45]. The delta function he describes is given by:

$$
\delta(\omega) = \lim_{\lambda\to\infty} \frac{\lambda}{\sqrt{\pi}} e^{-\lambda^2\omega^2} \tag{3.24}
$$

which reduces for $\beta = \lambda/\sqrt{\pi}$ to our definition of the delta function given by equation 3.23.

It is interesting to compare these results for other functions, which are often related to the Dirac delta function, e.g. $\lim_{\beta\to\infty} \beta \sin(\beta\omega)/(\beta\omega)$. To draw more conclusions about the delta function additional Fourier properties should be investigated and tested for the Gaussian shaped delta function. As the delta function is regarded as a Gaussian function, a hypothesis can be formulated that the oscillatory behavior associated with frequency shifted delta functions, i.e. $\delta(\omega - \omega_0)$, could be related to higher order derivatives of the delta function, i.e. Hermite type of functions.

3.4 Criteria on the basis set of signals

One of the most important parts of a communication system are the actual messages sent. In verbal communication these messages are referred to as a language. This section focuses on the design of a language for communication systems. The underlying hardware, which should create, transmit, receive and interpret the messages/words, is taken into account while designing the language.

Signal properties like linear independence, orthogonality and zero cross-correlation are regularly mentioned as necessities to establish communication, but arguments are often lacking. In case one of these conditions can be relaxed or omitted, new degrees of freedom are obtained which can result in a better or simplified communication system. Accordingly, this section discusses a comprehensive list of signal properties in relation to communication. The objective is to arrive at a set of criteria for a signal set for communication.

The following signal (set) properties are subsequently discussed:

- ◇ Continuity
- ◇ Linear dependence
- ◇ Orthogonality
- ◇ Correlation
- ◇ Energy
- ◇ Entropy
- ◇ Crest factor
- ◇ Localization
- ◇ Timing sensitivity
- ◇ Frequency sensitivity

The basis set of signals is indicated by S which contains N real signals s_i. The signal attributes and their importance in relation to communication are discussed below. To clarify signal properties like linear independence, orthogonality, orthonormality and uncorrelated signals, refer to figure 3.3. These signal attributes are discussed

Continuity | Signal s_1 is discrete if the signal is described by $\bar{s}_1$ with $\dim(\bar{s}_1) < \infty$
Although the signals in physical transceivers are analog, continuous time-varying signals, the signals are often generated, modulated and interpreted in the digital domain. The digital domain deals with signals sampled in time, called discrete time. Sampling may be performed uniformly or non-uniformly, although the latter poses significant difficulties for implementation. If the sampling rate and signal time-duration are limited, then the signals are described by vectors of limited dimension, i.e. $\dim(\bar{s}_i) < \infty$. Although a higher sampling rate offers a better approximation of continuous-time signals, the sampling rate is generally limited by the sampling rates of the Analog-to-Digital Converter (ADC) and Digital-to-Analog Converter (DAC). In addition lower sampling rates reliefs hardware requirements and lowers the power usage. To support the criterium of discrete time, signals s are presented from now on as vectors $\bar{s}$. Next to discrete time, the signals can also be discretized in amplitude by the process of quantization. Quantization introduces quantization noise as a result of rounding errors. As the effect of quantization can be limited by using small step sizes (small rounding errors), we do not take quantization into account

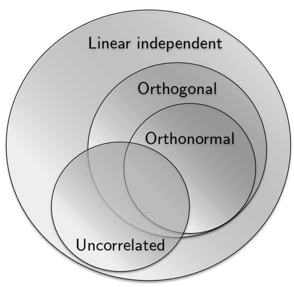

Figure 3.3 | Relations between linear independent, orthogonal, orthonormal and uncorrelated signals (based on [46]).

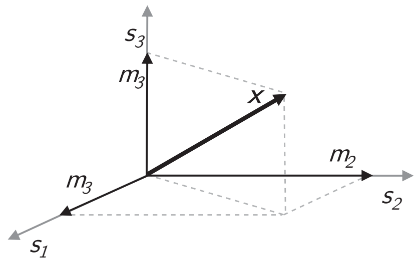

Figure 3.4 | A vector $\bar{x}$ finds itself in the Euclidean space spanned by signals $\bar{s}_1$, $\bar{s}_2$ and $\bar{s}_3$.

as a primary requirement for the design of target signal set S.
◇ *Criterium:* Signals $\bar{s} \in S$ should be in discrete time and are preferably uniformly sampled.

Linear dependence | $\bar{s}_1$ and $\bar{s}_2$ are linearly independent if there exists no $\alpha \in \mathbb{R}$ such that $\bar{s}_1 = \alpha \cdot \bar{s}_2$
When two signals $\bar{s}_1$ and $\bar{s}_2$ are transmitted simultaneously, their sum is described by $\bar{y} = \bar{s}_1 + \bar{s}_2$. If $\bar{s}_1$ is based on $\bar{s}_2$ by a linear relation like $\bar{s}_2 = \alpha \bar{s}_1$ then the receiver is uncertain about the information content contained in $\bar{y}$. The signal $\bar{y}$ can both be interpreted as $(1+\alpha)\cdot\bar{s}_1$ and as $(1/\alpha+1)\cdot\bar{s}_2$. The receiver is not able to indisputably distinguish the signals $\bar{s}_1$ and $\bar{s}_2$. For that reason we impose the constraint of linear independence for all signals $\bar{s}$ in the set of signals S.
◇ *Criterium:* Signals $\bar{s} \in S$ should be linearly independent and span an N-dimensional signal space.

Orthogonality | $\bar{s}_1$ and $\bar{s}_2$ are orthogonal if their inner-product $\langle \bar{s}_1, \bar{s}_2 \rangle = 0$
Assuming that the signals $\bar{s} \in S$ are linearly independent, the question arises whether the signals should be orthogonal. Let us assume the Euclidean space in $\mathbb{R}^3$ as visualized in figure 3.4 spanned by three signal vectors $\bar{s}_1$, $\bar{s}_2$ and $\bar{s}_3$. Any signal vector $\bar{x}$ can be constructed based on the signals $\bar{s}_1$, $\bar{s}_2$ and $\bar{s}_3$ by modulation with constants m_1, m_2 and m_3 respectively. The modulation and demodulation processes using signals S and information vector $\bar{m}$ can be seen as:

$$\bar{x} = \underbrace{\begin{bmatrix} s_{1_1} & s_{2_1} & s_{3_1} \\ s_{1_2} & s_{2_2} & s_{3_2} \\ s_{1_3} & s_{2_3} & s_{3_3} \end{bmatrix}}_{S} \cdot \begin{bmatrix} m_1 \\ m_2 \\ m_3 \end{bmatrix} \qquad \hat{\bar{m}} = \underbrace{\begin{bmatrix} s_{1_1} & s_{2_1} & s_{3_1} \\ s_{1_2} & s_{2_2} & s_{3_2} \\ s_{1_3} & s_{2_3} & s_{3_3} \end{bmatrix}^{-1}}_{S^{-1}} \cdot \begin{bmatrix} x_1 + n_1 \\ x_2 + n_2 \\ x_3 + n_3 \end{bmatrix} \tag{3.25}$$

whereby element s_{1_i} denotes the i[th] element of signal $\bar{s}_1$. $\hat{\bar{m}}$ is an estimate of $\bar{m}$ which is affected by additive noise $\bar{n}$. Now regard the following two example matrices describing the three signals $\bar{s} \in S$ and the corresponding inverses of these (non-singular) matrices:

$$\begin{aligned} S_1 &= \begin{bmatrix} 1 & 0 & 0 \\ 0 & 1 & 0 \\ 0 & 0 & 1 \end{bmatrix} & S_1{}^{-1} &= \begin{bmatrix} 1 & 0 & 0 \\ 0 & 1 & 0 \\ 0 & 0 & 1 \end{bmatrix} \\ S_2 &= \begin{bmatrix} 1 & 0.995 & 0 \\ 0 & 0.1 & 0 \\ 0 & 0 & 1 \end{bmatrix} & S_2{}^{-1} &= \begin{bmatrix} 1 & -9.95 & 0 \\ 0 & 10 & 0 \\ 0 & 0 & 1 \end{bmatrix} \end{aligned} \tag{3.26}$$

The signal sets S_1 and S_2 give two different estimates $\hat{\bar{m}}$:

$$\hat{\bar{m}}(S_1) = \begin{bmatrix} m_1 \\ m_2 \\ m_3 \end{bmatrix} + \begin{bmatrix} n_1 \\ n_2 \\ n_3 \end{bmatrix} \qquad \hat{\bar{m}}(S_2) = \begin{bmatrix} m_1 \\ m_2 \\ m_3 \end{bmatrix} + \begin{bmatrix} n_1 \\ \sqrt{9.95^2 + 10^2} \cdot n_2 \\ n_3 \end{bmatrix} \tag{3.27}$$

It is apparent that signals S_2 are performing worse than signals S_1, because the noise is considerably amplified. The explanation lies in the fact that the signals $s_1 = [1\ 0\ 0]$ and $s_2 = [0.995\ 0.1\ 0]$ of set

S_2 are nearly equal. The matrix is said to be ill-conditioned. Singular matrices have an infinite condition number while the best-conditioned matrices have a condition number of 1. A condition of 1 does not lead to a degradation of the SNR as is the case for signals S_2. The condition number of 1 is only achieved by a perfectly orthogonal set [47].

In brief, a signal set is optimal for noise when the signals in the set are orthogonal. Note that orthogonality is not strictly necessary, but desired to achieve energy-efficient communication in additive noise channels. The fact that orthogonality is not a strict necessity is also mentioned by Kozek and Molish [48]. They state that wireless systems are rarely limited by their AWGN performance. Thus, eliminating ISI and ICI is often more important. It can be advantageous to drop the orthogonality constraint in order to obtain extra freedom to design signals which are more robust against time- and frequency dispersion. Despite the notice that orthogonality is not strictly necessary, orthogonality is still an attractive property for the signals $\bar{s} \in S$ because of its mathematical convenience and for its performance in AWGN channels.
◇ *Criterium:* Signals $\bar{s} \in S$ are preferably orthogonal.

Correlation | $\bar{s}_1$ and $\bar{s}_2$ are uncorrelated if $\langle\, \bar{s}_1 - E(\bar{s}_1), \bar{s}_2 - E(\bar{s}_2)\,\rangle = 0$
As a measure for correlation between two signals the correlation definition as defined in [46] is used stating: $\langle\, \bar{s}_1 - E(\bar{s}_1), \bar{s}_2 - E(\bar{s}_2)\,\rangle = 0$ whereby $\langle .. , .. \rangle$ refers to the inner-product and $E\,(..)$ resembles the expectation value. The property of correlation becomes the criterium of orthogonality in case we deal with signals of zero-mean, i.e. $E(\bar{s}_i) = 0$. A zero-mean signal is desired to prevent DC (read: very low frequency) components in the analog building blocks. Assume for example a DC component which is mixed to f_{osc} in the transmitter. The signals received by the receiver are in the order of microvolts and a small (capacitive or substrate) coupling with the Local Oscillator (LO) results in substantial energy centered at $f = f_{osc}$ [49]. The DC component of the signal set is situated at the same frequency bins and is likely to be indistinguishable from the LO-coupled signal. In addition, because of the energy concentration around f_{osc}, we even risk that the DC component is filtered out to prevent saturation of the subsequent amplifying stages.
A solution may be found by making sure that modulation is a zero-mean process with constellations around the origin. However, there are still low frequency components if similar symbols are consecutively transmitted. Therefore, we pose the requirement that the signals $\bar{s} \in S$ are zero-mean, i.e. $E(s_i) = 0$. The correlation property now simplifies to the orthogonality condition, which was already discussed.
◇ *Criterium:* Signals $\bar{s} \in S$ should be zero-mean

Energy | $\bar{s}_1$ and $\bar{s}_2$ have equal energy if $\|\bar{s}_1\|^2 = \|\bar{s}_2\|^2$
If the transmitter, channel and receiver affect signals $\bar{s}_1$ and $\bar{s}_2$ in the same way the signal impairments are equal and the expected SNRs at receiver side are likely to be equal in case the signals $\bar{s}_1$ and $\bar{s}_2$ contain the same amount of energy. Consequently, the probabilities of correct interpretation of the received signals $P(\bar{s}_1|\hat{\bar{s}}_1)$ and $P(\bar{s}_2|\hat{\bar{s}}_2)$ are the same. In general equal probabilities are desired. If either the influence of transmitter, channel and receiver is signal dependent or if one signal is more important than another, the requirement of equal energy signals can be omitted and changed accordingly. In case we deal with both orthogonal and equal energy signals, the term orthonormality applies to the set of signals, see figure 3.3.
◇ *Criterium:* Signals $\bar{s} \in S$ have preferably equal energy.

Entropy | Let $\bar{s}_1'$ be an amplitude modulated version of $\bar{s}_1 \in S$. If $\bar{x}$ is constructed by modulating several basis signals $\sum_{n=1}^{N} \bar{s}_n'$ then an element $x_i \in \bar{x}$ is assumed to have a random amplitude and the differential Shannon entropy is given by $H = -\int p(z)\log_2(p(z))dz$ with $p(z)$ the PDF of x_i.
We aim at a set of signals which comprise a lot information. This means that the signals should have the possibility to behave in an unexpected way. Namely, the expected is already expected and does not need to be transmitted. For the information-richness of a signal or a set of signals S we use the Shannon-type of entropy for random variables with continuous Probability Density Functions (PDFs) [11].

> ◇ **What's in a name?**
> There are not many terms which have as many definitions as entropy. Although we limit ourselves to the Shannon entropy, even this entropy knows several versions. In addition, Shannon interchanges terms like information, uncertainty and entropy in his classical work [11]. A former MIT director, Tribus, asked Shannon what he thought of when he coined the term entropy. Shannon's response was:
> *"My greatest concern was what to call it. I thought of calling it 'information', but the word was overly used, so I decided to call it 'uncertainty'. When I discussed it with John von Neumann, he had a better idea. Von Neumann told me, 'You should call it entropy, for two reasons. In the first place your uncertainty function has been used in statistical mechanics under that name, so it already has a name. In the second place, and more important, no one knows what entropy really is, so in a debate you will always have the advantage"* [50].

Modulation of signal $\bar{s}_1$ with some constant m_1 gives a modulated version $\bar{s}'_1$. Next to $\bar{s}_1$, all other signals $\bar{s}_{2..N}$ can be modulated by constants $m_{2..N}$. This gives a set of modulated signals $\bar{s}'$ which add up to $\bar{x}$, i.e. $\bar{x} = \sum_{k=1}^{N} \bar{s}'_k$. An individual element of $\bar{x}$ at a distinct time i has an amplitude described by the sum of all i^{th} elements of the modulated signals $\bar{s}'$. As the amplitude x_i is the sum of many modulated signals $\bar{s}'$ at time instant i the PDF of x_i can be approximated by a continuous distribution. Therefore we use the continuous (differential) entropy definition.

> ◇ **Power limited versus Energy limited**
> The question arises what kind of signal contains the highest entropy. We propose to distinguish power-limited and energy-limited signals. First, in case we deal with a power-limited signal, the power of the random signal x_i under the assumption of a unit time, given by $|x_i|^2$, is limited in its power to a certain power level P. In that case the integration interval for the entropy H is limited to the interval $-\sqrt{P} \leq z \leq \sqrt{P}$. The maximum entropy yields now a uniform distribution [11]. The PDF for $p(z)$ is then given by $1/(2\sqrt{|P|})$ and gives a maximum (differential) signal entropy of $\log_2(2\sqrt{|P|})$.
> Second, when the power of the signal is unbounded and we restrict only the energy of the signal, then we (theoretically) allow for the power P to be infinite. The integration interval for the entropy H is now $[-\infty, \infty]$ and according to [11] the maximum entropy is then given for a Gaussian distributed PDF $p(z) = 1/(\sqrt{2\pi}\sigma)e^{-z^2/(2\sigma^2)}$. The entropy for a Gaussian shaped PDF with a standard deviation σ is $H = \log_2(\sqrt{2\pi e}\sigma)$. When the set of signals S_N is large (like generally in multi-carrier systems) then under the central limit theorem (and fulfilling corresponding criteria), the PDF of the random amplitude tends to a Gaussian distribution. So, when the signal $\bar{x}$ is constructed by the modulated signals $\bar{s}$, then the PDF of an element x_i is expected to approach a Gaussian distribution when $N \to \infty$.

Setting a limit on the signal power P gives a maximum signal (differential) Shannon entropy of $\log_2(2\sqrt{P})$. Without a power constraint, the maximum entropy achievable is given by $\log_2(\sqrt{2\pi e}\sigma)$ with σ the standard deviation of the PDF of the amplitude. In that case a higher entropy is achieved than for the power-limited case, but at the cost of high power peaks. For example, for a Gaussian-shaped PDF of the random variable x_i there is 0.3% chance on a signal power of $(3\sigma)^2$.
◇ *Criterium:* The PDF of the random amplitude of signal $\bar{x}$ based on $\bar{s} \in S$ should be Gaussian shaped.

Crest factor | PAPR of signal $\bar{x}$, based on signals $\bar{s} \in S$, is $\left|x_{peak}\right|^2/|x_{rms}|^2$
Energy and power are related, but they form different criteria on the set of signals $\bar{s} \in S$. Where the energy of the signals is spread over time and frequency, the power is specified for a certain moment in time (or a specific frequency). A high crest factor, or similarly a high Peak to Average Power Ratio (PAPR), requires a high dynamic range of the transceiver building blocks. But a high PAPR may also indicate - under the assumption that the signal set is well-constructed - high-entropy signals. Therefore we stick to the entropy-condition and do not incorporate PAPR restrictions. At runtime, clever constellation mappings may lower the PAPR and as discussed also lower the entropy of the transmitted signals.
◇ *Criterium:* Signals $\bar{s} \in S$ are not restricted in peak power.

Time & frequency localization | $\min(\sqrt{\sigma_T^2 \cdot \sigma_F^2})$ with σ_T^2 and σ_F^2 defined as in chapter 2.
Efficient communication in a spectrum-scarce environment is achieved when spectral users limit their mutual interference while achieving high datarates. This can be realized by signals which are localized in

time and frequency. The aspect of time-frequency localization has been the primary topic of chapter 2. As our goal is to find a solution to spectral leakage in multi-carrier systems, it may be clear that time & frequency localization is an important criterium for the signals $\bar{s} \in S$.
⋄ *Criterium:* Signals $\bar{s} \in S$ should be localized in time & in frequency.

Time & Frequency sensitivity
If the signals $\bar{s} \in S$ are transmitted, the signals propagate as electromagnetic radiowaves through some medium. Mobile radio channels are characterized by time- and frequency dispersion caused by multi-path effects and Doppler spreads (discussed in chapter 4), which are likely to cause ISI and ICI. Robustness against multi-path effects, timing jitter, Doppler spreads, frequency offsets and phase noise is desired.
⋄ *Criterium:* The signals $\bar{s} \in S$ should possess some robustness against time- & frequency deviations.

3.5 Assessment of the Hermite functions

The previous section discussed signal properties in order to arrive at a set of criteria for a basis set of signals S for communication. A short summary of the discussed criteria is given below. Signals $\bar{s} \in S$:
- ⋄ should be in discrete time and preferably uniformly sampled
- ⋄ should be linear independent
- ⋄ are preferably orthogonal
- ⋄ should be zero-mean
- ⋄ have preferably equal energy
- ⋄ have a Gaussian shaped PDF for their modulated sum $\bar{x}$
- ⋄ are not restricted in their peak power
- ⋄ should be localized in time & frequency
- ⋄ should possess some robustness against time & frequency deviations

Table 3.5 discusses the performance of the probabilistic Hermite functions with regard to the stated requirements. Note that a number of criteria are not or not fully met. Based on their excellent localization property, we still propose to elaborate on the Hermite functions. Modifications are necessary in order to have a suitable set of signals for communication, which are discussed in upcoming sections.

3.6 Modification of the Hermite based signals

The previous section assessed the suitability of Hermite functions for communication. Challenges are the sampling of the continuous-time Hermite functions, truncation of the symbol-duration and symbol-bandwidth, and obtaining uncorrelated zero-mean signals.

3.6.1 Discretization

The signals $he_n(t)$, as discussed so far, are continuously varying over time. We aim for a signal set S with time-discrete signals. That corresponds to finding the optimal sampling points such that the signal characteristics are not severely degraded. The issue of sampling functions has been addressed by Nyquist and Shannon by their sampling theorem, but their theory is based on band-limited signals. They state that the (Nyquist) sampling rate should be larger than two times the bandwidth, i.e. $f_s > 2BW$. In chapter 2 we already left the assumption of strict band-limited signals. Namely, the Hermite functions stretch over the bandwidth $[-\infty, \infty]$ and treating the signals as band-limited would be disputable.

For sampling the Hermite functions we explore the field of numerical integration. Note that orthogonality and correlation of signals involve the integral over two, possibly shifted, signals. While the continuous time deals with integrals, discrete time only evaluates the signal values at distinct moments in time. In order for the orthogonality of the Hermite functions to hold, the correct sampling instants

Requirement	Performance	Comments
Discrete time	-	The Hermite functions are in continuous time. The waveforms need to be discretized, preferably by uniform sampling, such that the elementary signal properties are not severely degraded.
Linear independent	+++	The Hermite functions satisfy the requirement of linear independence. Each function he_n contains a polynomial of degree n which cannot be written as a linear sum of the other polynomials.
Orthogonality	+	As discussed in the previous section, the Hermite functions are orthogonal over the interval $[-\infty, \infty]$. This gives a paradox as the signals are non-causal & orthogonal or causal & non-orthogonal. Thanks to the rapid decay of the functions (by the term $e^{-t^2/4}$) the values rapidly become negligibly small such that the loss of orthogonality becomes insignificant. In relation to orthogonality in time and frequency, attention should be paid to the truncation of symbol time T_s and symbol bandwidth BW_s.
Zero-mean	- -	Although the Hermite functions are an orthogonal set of signals that does not automatically mean that the functions are uncorrelated (according to the Pearson's correlation product). When the signals are zero-mean the correlation condition simplifies to the orthogonality condition, but not all Hermite functions possess the property of zero-mean. All even Hermite functions, i.e. he_n with $2n \in \mathbb{N}_0$, have a non-zero mean over the interval of interest $[-T_s, Ts]$ with T_s limited in time. To achieve the requirement of non-correlated signals the signals should be transformed such that the signals become zero-mean while still satisfying the orthogonality restraint.
Equal energy	+	The Hermite functions need to be normalized correctly in order to deal with equal energy signals. The constraint is relatively easy satisfied.
High entropy	++	Based on simulations, we known that the sum of N modulated Hermite functions is Gaussian distributed when N is relative large. This implies that we deal with a high entropy transmit signal. The high entropy is achieved at the cost of an unconstrained PAPR.
Localization	+++	The Hermite functions are the solutions for optimal time-frequency localization as discussed in chapter 2. Accordingly, the functions satisfy the requirement of time and frequency localization. Attention should be paid to the sphere-packing problem: how to efficiently assign time-slots and frequency bands to multiple users.
Timing sensitivity		*To be investigated**
Frequency sensitivity		*To be investigated**

Table 3.5 | Assessment of the Hermite functions based on the set requirements for communication signals. The performance indicators +++, ++, +, +/-, - and - - are relative measures to indicate the easiness versus difficulties for Hermite functions to meet the listed requirements. ** The importance of these criteria are acknowledged, but has not been taken into account in the design of the signals $\bar{s} \in S$.*

need to be found. Gauss formulated an approximation over finite elements K in order to approximate a continuous function $s(t)$:

$$\sum_{k=1}^{K} w_k s(t_k) \approx \int_{t_0}^{t_e} s(t)dt \quad w_k \in \mathbb{R} \; t_k \in \{t_0, \dots, t_e\} \tag{3.28}$$

which is referred to as the general Gaussian quadrature rule. The Gaussian-Hermite quadrature rule is a specific quadrature rule addressing the integration points t_k, called abscissae, and weight factors w_k for Gaussian weighted polynomials $s(t)$ [51]:

$$\sum_{k=1}^{K} w_k s(t_k) \approx \int_{-\infty}^{\infty} e^{-t^2} s(t)dt \tag{3.29}$$

The domain of integration for the Hermite function stretches over $[-\infty, \infty]$ and the integration yields good results for polynomials up to degree $2K - 1$ (keeping their mutual orthogonality). Nevertheless, to distinguish N different hermite functions at least K sampling points are necessary, so $K \geq N$. The abscissae t_k are given by the zero-crossings of the polynomial of $He_n(t)$. The abscissae are the same for the probabilistic and physicist Hermite functions. As we are primarily interested in sampling the func-

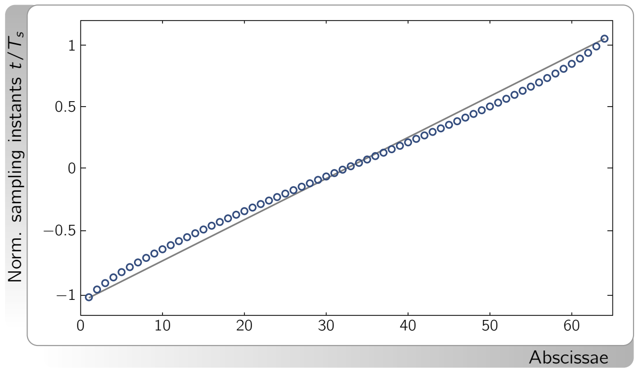

Figure 3.5 | Normalized sampling instants according to Gaussian-Hermite quadrature rule for $N = 64$. The linear line (gray) indicates uniform sampling while the optimal sampling points according to the quadrature rule (o) slightly deviate from this line indicating the need for non-uniform sampling.

tions, the abscissae t_k are used to determine the sampling points of the continuous time function $he_n(t)$ (not weights are aplied). Note that applying the correct weights may yield a better result. Leibon e.a. advocate the Newton-Cotes quadrature formula giving other points for the abscissae [52]. Nevertheless we use the abscissae from the Gaussian quadrature rule. The abscissae values for $K = 64$ are shown in figure 3.5. Note that the abscissae for other values of K are different. In case one would only use $N = 32$ still the abscissae for $K = 64$, but now two times more samples are used than strictly necessary.

As uniform sampling significantly eases implementation, we propose to scale the signals s_i in time according to the abscissae distribution t_i. The signals are now slightly distorted, a bit less ideal, but also more convenient for engineers. The Hermite functions he_n are from now on, unless otherwise stated, vectors $\overline{he}_n$ of dimensionality N sampled at the distinct times t_i.

3.6.2 Orthogonality & Uncorrelated

The cornerstone of the Hermite functions are the Hermite polynomials He_n. Let us consider a contradiction related to the orthogonality and zero-mean requirement. On one hand, the probabilists' Hermite polynomials become orthogonal by applying the weighting function $e^{-t^2/4}$, but then the product is not zero-mean. On the other hand it was found that by applying a weighting function $e^{-t^2/2}$ the product becomes zero-mean, but is not orthogonal anymore.

In literature authors deal differently with the problem. Haas and Belfiore, who designed a pulse-shaping prototype filter, select only the odd Hermite functions which have zero-mean [53]. Chongburee did design an antipodal Hermite transmission system, did not meet the requirement of zero-mean, and noticed that the non-zero cross-correlation of Hermite functions caused failure of the designed Maximum A Posteriori (MAP) receiver [54]. For Ultra-Wideband (UWB) pulse-shaping some authors did take the zero-mean condition into account and proposed shape-modification methods for the Hermite functions [55], [56] and [57]. Ghavami e.a. [55] change the basis by introducing a sinusoidal signal such that we cannot speak of true Hermite functions. In fact, they get signals similar to Gabor frames which are exponentially weighted complex exponentials. [57] and [56] were using quite extensive methods leading to modified Hermite functions of low degree with a high number of zero crossings (effectively changing their degree). Especially the approach of da Silva and Campos [56] as they optimize to get more wide-band pulses (possibly more robust against frequency dispersion), but their approach is quite elaborate and effectively changes the degree of the Hermite functions.

We propose a relatively simple method which keeps the degree n of the Hermite functions he_n the same (so minimally changing the shape and complexity of the signals) and aims at achieving zero-mean, orthogonal signals. The zero-mean property also leads to satisfying the criterium of uncorrelated signals.

Finally, applying a normalization satisfies the criterium of equal energy.

Using the Hermite functions $\overline{he}_n(x)$ with a (second) weighting function $e^{-x^2/4}$, it is found and easily verified that the product has a zero mean. Obvious exception is the Hermite function of degree 0 as it does not have a zero crossing and always has a non-zero mean. Assume a set of N Hermite functions $\overline{he}_n(x)$ of degree $n > 0$ with zero mean:

$$\overline{he}_{zm} = \begin{bmatrix} e^{-x^2/4} \cdot \overline{he}_1(x) \\ e^{-x^2/4} \cdot \overline{he}_2(x) \\ \vdots \\ e^{-x^2/4} \cdot \overline{he}_N(x) \end{bmatrix} \tag{3.30}$$

The vector $\overline{he}_{zm}$ contains zero-mean, but non-orthogonal signals. We apply the Gram-Schmidt Orthogonalization method on the vector $\overline{he}_{zm}$. The first signal $\bar{s}_1$ is simply equal to $he_{zm,1}$. The second signal $\bar{s}_2$ is now the second signal $he_{zm,1}$ minus its projection on the first orthogonal signal $\bar{s}_1$. The projection is calculated by the inner-product. This process can be mathematically described by:

$$\begin{bmatrix} \bar{s}_1 \\ \bar{s}_2 \\ \bar{s}_3 \\ \vdots \\ \bar{s}_N \end{bmatrix} = \begin{bmatrix} e^{-x^2/4} \cdot \overline{he}_1 \\ e^{-x^2/4} \cdot \overline{he}_2 \\ e^{-x^2/4} \cdot \overline{he}_3 \\ \vdots \\ e^{-x^2/4} \cdot \overline{he}_N \end{bmatrix} - \begin{bmatrix} 0 & 0 & 0 & \cdots & 0 \\ \frac{\langle \bar{s}_1, e^{-x^2/4}\overline{he}_2 \rangle}{\|\bar{s}_1\|^2} & 0 & 0 & \cdots & 0 \\ \frac{\langle \bar{s}_1, e^{-x^2/4}\overline{he}_3 \rangle}{\|\bar{s}_1\|^2} & \frac{\langle \bar{s}_2, e^{-x^2/4}\overline{he}_3 \rangle}{\|\bar{s}_2\|^2} & 0 & \cdots & 0 \\ \vdots & \vdots & \ddots & \cdots & 0 \\ \frac{\langle \bar{s}_1, e^{-x^2/4}\overline{he}_N \rangle}{\|\bar{s}_1\|^2} & \frac{\langle \bar{s}_2, e^{-x^2/4}\overline{he}_N \rangle}{\|\bar{s}_2\|^2} & \cdots & \frac{\langle \bar{s}_{N-1}, e^{-x^2/4}\overline{he}_N \rangle}{\|\bar{s}_{N-1}\|^2} & 0 \end{bmatrix} \cdot \begin{bmatrix} \bar{s}_1 \\ \bar{s}_2 \\ \bar{s}_3 \\ \vdots \\ \bar{s}_N \end{bmatrix} \tag{3.31}$$

Equation 3.31 is suitable for numeric evaluation in an iterative way. To get an orthonormal vector the values $\bar{s}_n$ (after calculation of equation 3.31) can be divided by their norms $\|\bar{s}_n\|$. Hereby we also meet the requirement of orthonormality and thus equal energy signals.

We constructed a set of orthogonal signals S which are a sum of weighted Hermite functions. As every function $\overline{he}_{zm}$ is zero-mean their sums are also zero-mean. In addition each signal $\bar{s}_n$ is of degree n or lower in contrast with the approach used by [56]. Signals $\bar{s} \in S$ constructed by low order Hermite functions are preferred as they occupy less time and bandwidth than the higher order Hermite functions. The Hermite functions of degree 1 to 5 are reprinted in figure 3.6 while the modified signals are shown in figure 3.7. Notice the lack of a DC component in figure 3.7.

Summarizing, this chapter started with a short treatment of Hermite polynomials and functions. Afterwards, ten signal properties were discussed leading to the formulation of criteria for a basis set of communication signals. Based on these criteria the Hermite functions were assessed and subsequently modified to comply with all criteria. The resulting signals $\bar{s} \in S$ are in discrete time, linearly independent, orthogonal, uncorrelated, have equal energy, can be used for maximum entropy transmit signals and are localized in time- and frequency. In upcoming sections these time-frequency localized signals are referred to as S_{TFL}. No power constraint has been taken into account as it trades off with entropy. It is recommended for future work to analyze the sensitivity of a set of Hermite functions for timing and frequency deviations. The next chapter assesses the performance of the signals S_{TFL}.

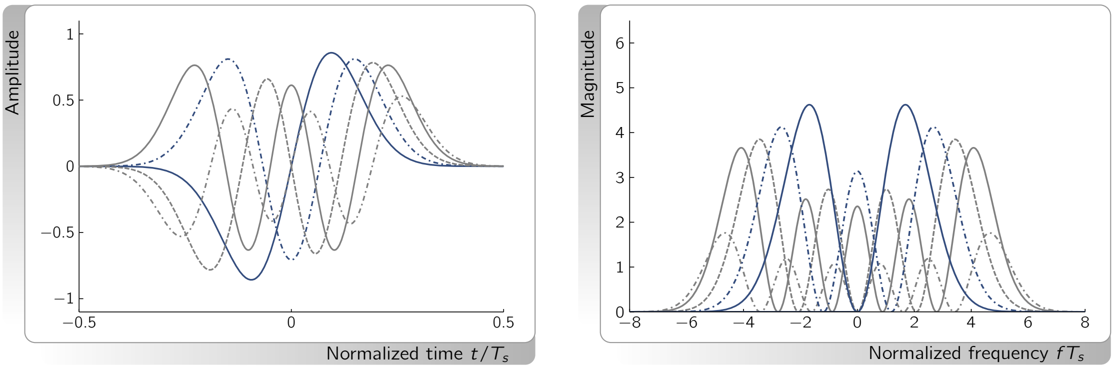

Figure 3.6 | Five probabilistic Hermite functions of degree 1..5: time (left) and frequency (right) representations (plot generated using a slightly higher sampling rate).

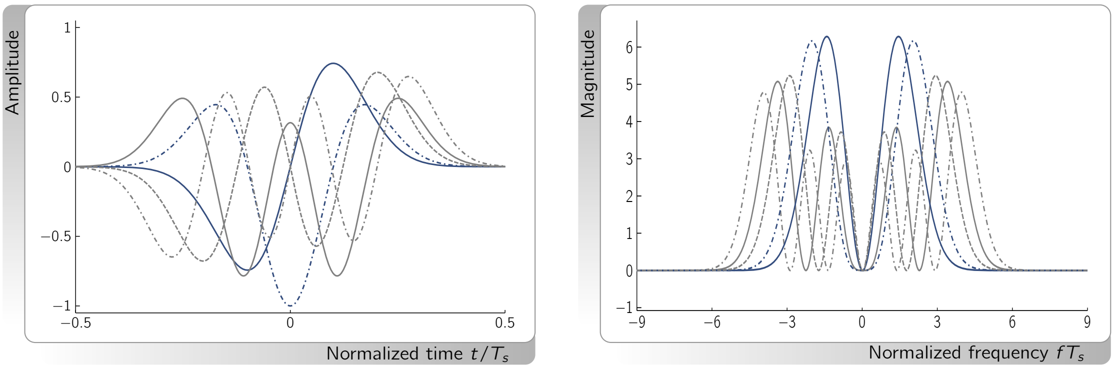

Figure 3.7 | Five proposed signals S_{TFL} of degree 1..5: time (left) and frequency (right) representations (plot generated using a slightly higher sampling rate).

CHAPTER 4

Performance Assessment

The previous chapter led to a set of time-frequency localized signals S_{TFL}, which has been designed based on formulated signal criteria for communication. One may pose the proposition that the signal set S_{TFL}, as designed in chapter 3, is a suitable signal basis for communication. Such a proposition asks for verification, ideally by a real-world system, or at least by simulations of relevant performance measures. This chapter first discusses performance measures to be evaluated. Afterwards, a short overview of the transmitter, channel and receiver setups is given. A number of standard simulations are carried out to get insight in achievable datarates, in multi-user communication and the performance in mobile radio channels. Next to the effectiveness also the efficiency of the communication system, in terms of power and complexity, is discussed.

4.1 Performance measures

In contrast with chapter 3, this chapter analyzes system performance rather than signal properties. The aim of this research is to reduce spectral leakage while maximizing the effective data transfer rate and staying within energy, bandwidth and complexity budgets. The achievable datarates in single-user and multi-user cases are discussed. Simulation of the Bit Error Rates (BERs) for different mobile radio channels gives an impression of the robustness of the signal set S_{TFL} for noise and fading.
Next to the effectiveness of the transceiver, i.e. achieving high datarates with low BERs, also the efficiency is regarded. From a signal perspective the crest factor / PAPR has not been included as a requirement, because it trades off with entropy. Nevertheless, from a system perspective, it is relevant to know the likelihood of certain power peaks to determine the dynamic range requirements. In addition, a pragmatic overview of the hardware requirements for transmitter and receiver building blocks is given. Rather than an exhaustive treatment, a short overview of hardware implications is presented based on a comparison between S_{TFL} and conventional OFDM signals.

Summarizing, this chapter focuses on system performance criteria targeting both the effectiveness and efficiency of a communication system employing signals S_{TFL}:

- ◇ Datarates
- ◇ Multi-user communication
- ◇ Bit Error Rates
- ◇ Peak to Average Power Ratio
- ◇ Transmitter complexity
- ◇ Receiver complexity

4.2 Transceiver & Simulation setup

In order to judge the performance of S_{TFL}, a reference is needed. The 802.11 standard, better known as Wi-Fi for WLAN, is a well-known OFDM standard. We loosely base the simulations on IEEE 802.11 amendment a/g. Documentation can be found in the corresponding IEEE 802.11 standards [58], [59] and [60]. The simulation parameters for a standard sinusoidal OFDM transmission system and a transmission system based on the signals S_{TFL} are given in table 4.1. Because numerical evaluation of Hermite functions suffers from significant inaccuries for degree 48 and higher, we choose to limit the set of active carriers to 42. Working with higher precision arithmetic and/or cleverer algorithm implementations may solve the problem. As we do not regard this as a major problem, it is outside the scope of this research and we simply limit the number of active carriers.

The simulation is performed using MathWorks Matlab and consists of a number of blocks in order to resemble actual transceivers dealing with signals S_{TFL}. The transceiver blocks are shortly described.

The transmitter
The transmitter building blocks and simulations steps are as follows:
1. A serial datastream of $\geq 10^5$ random bits is generated.
2. Depending on the chosen modulation (BPSK, 4PAM or 8PAM) the stream is split into blocks of respectively 1, 2 or 3 bits which are fed in parallel to the modulator.
3. The modulator uses the signals S_{TFL}, as described in chapter 3: discretized, scaled, zero-mean, orthogonal signals based on Hermite functions. As the total number of carriers is 54, we have also 54 discrete time (uniform)

Specification	802.11	OFDM*	S_{TFL}	Units
Number of carriers (1)	64	54	54	
Modulated carriers (2)	52	42	42	
Pilot symbols (3)	4	4	4	
Bandwidth (4)	20	16.875	16.875	MHz
Carrier spacing (5)	0.3125	0.3125	N/A	MHz
Active symbol duration (6)	3.2	3.2	3.2	us
Guard / Cyclic prefix (7)	0.8	0.8	0	us
Symbol duration (8)	4.0	4.0	3.2	us
Coding rate (9)	$\frac{1}{2} \cdots \frac{3}{4}$	1	1	
Modulation (10)	64QAM	BPSK / 4PAM / 8PAM		
		QPSK / 16QAM / 64QAM (I&Q)		
Bitrate (11)	54	$9.5 \cdots 28.5$	$11.875 \cdots 35.625$	Mbit/s
		$19 \cdots 57$	$23.75 \cdots 71.25$	Mbit/s

Table 4.1 | Simulation parameters based on 802.11a/g parameters for comparison between OFDM* signals and signal set S_{TFL}. When quadrature modulation is applied, the number of carriers per bandwidth and bitrates are doubled. The bitrates are calculated by $\underline{11} = (\underline{2} - \underline{3})/\underline{6} \cdot \underline{9} \cdot \log_2(\underline{10})$ with $\underline{10}$ equals 2 for BPSK, 4 for 4PAM etcetera.

samples over time. As 802.11a/g does not use all carriers for sending data, we exclude the 12 signals S_{TFL} of highest degree.

4. The 42 data carriers are modulated dependent on the used modulation: BPSK, 4PAM or 8PAM. The constellation points are placed such that the average 'energy' of the constellations is unity.

5. The modulated signals $\bar{s} \in SS_{TFL}$ are added together (over time) to form the transmit signal $\text{tx}(t)$.

6. The transmit signal subsequently leaves the DAC as a zero-order hold signal and is mixed to the carrier frequency. As AM is known to be spectrally inefficient, quadrature modulation is applied. Modulation of an in-phase (I) and out-of-phase (Q) set of Hermite signals and subsequent I&Q mixing to the carrier frequency f_c effectively reduces the bandwidth per carrier by a factor 2. The principle of quadrature modulation relies on the multiplication of an in-phase set of (real) signals by $\cos(2\pi f_c t)$ and a quadrature set of (real) signals by $-\sin(2\pi\omega_c t)$. These sets are separable at the receiver thanks to the orthogonality of the $\cos(2\pi f_c t)$ and $\sin(2\pi f_c t)$ terms. Refer for more information to [49] or [61].

7. Finally the signal is amplified and transmitted. Stages 6 and 7 are assumed ideal in the simulation.

The channel

Leaving the transmitter, we deal with propagating electromagnetic waves, which are degraded by noise and distorted due to time-dispersion (e.g. multi-path effects) and frequency-dispersion (e.g. Doppler-shift). The first set of simulations degrade the signal waveforms with AWGN. The second set of simulations also takes slow & frequency selective fading into account. AWGN and fading form the primary topics of sections 4.5.1 and 4.5.2. The transmit signal $\text{tx}(t)$ is convolved with the fading channel response and the signal is subsequently degraded by AWGN. The received signal is referred to as $\text{rx}(t)$.

The receiver

The receiver is assumed to know the channel response, which can be realized by pilot symbols, channel estimation and by the assumption of a slowly varying channel.

1. The received signal $\text{rx}(t)$ is amplified by a Low Noise Amplifier (LNA), mixed to baseband to an in-phase and quadrature part by an I&Q mixer and discretized and quantized by an ADC. We obtain two sets of real signals representing the in-phase and quadrature set.

2. The in-phase (and quadrature) signals are equalized. The simulation assumes a perfect equalization (in time or frequency) based on the known channel response.

3. The digitized signal is evaluated by matched filters such that the 'correlation' between transmit signal and basis functions S_{TFL} becomes known. A correlation receiver would calculate cross-correlations and evaluate the output at distinct moments in time T_s. It can be deduced that the correlator-output at T_s is equal to the output of a matched filter, which calculates only one inner-product per symbol time [61]. Synchronization is a prerequisite in order to prevent ISI and is assumed to be perfect.

4. Subsequent demodulation of these 'correlations' recovers sent information. Demodulation is based on the modulation applied in the receiver: BPSK, 4PAM or 8PAM.

5. The blocks of bits are converted into a serial stream representing the original bit-stream, typically with some

bit-errors due to the signal degradation caused by the channel.

Although the introduction of more non-idealities seemingly results in a better approximation of the real-world performance, it makes it harder to carry out comparisons with literature. Assumptions of perfect channel estimation, equalization and synchronization are regularly encountered. Nevertheless, it is recommended to carry out more extensive simulations whereby more non-idealities are taken into account. In the end the best performance assessment is achieved by evaluating the performance of a real wireless transceiver system employing signals S_{TFL}.

4.3 Datarates

In previous sections no strict bandwidth definition has been given. Chapters 2 and 3 dealt with time- and frequency variances instead of absolute time durations and bandwidth definitions. In order to analyze datarates as function of time and bandwidth, definitions are required. The exhibit addresses this point.

> ◇ **On the application of the Shannon limit**
> The Shannon limit has been a driving force for the telecommunications industry during last decades. The Shannon theorem relates the achievable datarate in a channel to the signal power, noise level and bandwidth and has challenged researchers and engineers to achieve datarates close to the Shannon limit.
>
> The fundamental work of Shannon [11] discusses the achievable datarates for band-limited signals. The Shannon limit in its simple form is heavily based upon the Nyquist and Shannon sampling theorem stating that the sampling rate for a bandlimited signal of bandwidth BW should be $f_s > 2BW$. We already noticed that for signals of infinite bandwidth, as for our signals S_{TFL}, the Shannon and Nyquist sampling theorem does not suffice as it implies an infinite sampling rate. As the sampling theorem does not apply for our case, we may question the applicability of the Shannon limit.
>
> The Shannon limit is useful for describing the channel capacity, but not adequate for describing datarates for our signals S_{TFL}, for two reasons. First, the signals S_{TFL} are unlimited in time and bandwidth. Any treatment as limited in time or frequency would be disputable. It can be argued that a solution is formed by an approximation of the signals by a large number of band-limited signals. Although it is a practical solution, an analytical expression valid for non-strictly band-limited signals is preferred. Second, when the non-band limited signals are approximated by a band-limited signal (like by the common usage of the pass-band bandwidth), it does not provide any information regarding the amount of energy outside the bandwidth. This is relevant in a multi-user case. For example if several users are using time-limited, unfiltered, Fourier basis signals in a fairly limited bandwidth the users are likely to cause large amounts of mutual interference due to OFDM sidelobes, leading to bit errors, retransmissions, and finally dropping all datarates far below the Shannon limit.
>
> In chapters 2 and 3 we expressed the signals in terms of spread/variance in time and frequency according to the uncertainty principle definitions. Similarly, we proposed to write the number of bits as a function of spread of energy (e.g. higher order moments, uncertainty) in time and frequency, power and noise merely than as a function of time, (passband) bandwidth, power and noise. This would give a meaningful tool to analyze signals which are not strictly band-limited and provides insight in achievable datarates in multi-user cases.

As a practical solution, a bandwidth (and similar time duration) definition for no band- nor time-limited signals is necessary. In order to facilitate comparisons with literature and FCC guidelines, dBc bandwidth definitions can be used. A -60 dBc definition indicates the point where the power in an adjacent channel divided by the power in the channel carying the information signal is -60 dB, measured over a certain bandwidth, e.g. 100kHz. Independent of the chosen dBc definition, the bandwidth definitions are somewhat arbitrary as infinite number of BW_{dBc} points can be identified. Despite this observation, in order to conform to the FCC guidelines and to obtain time-bandwidth comparisons of the signals S_{TFL} with the conventional Fourier basis, we choose 3 points to define the symbol bandwidth and symbol time durations. First, the point where the S_{TFL} or OFDM siganls are maximum and start to decay (exponentially), referred to as a 0dBc point. Second, the -60dBc point is chosen to serve the FCC requirements

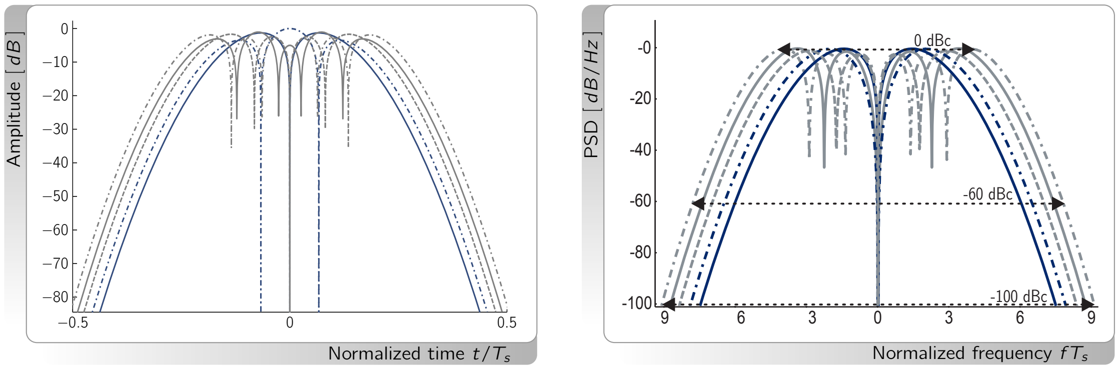

Figure 4.1 | Five signals S_{TFL} of lowest degree: logarithmic time (left) and frequency (right) representations. Notice the fast decay both in time and frequency of the signals. The 0dBc, -60dBc and -100dBc bandwidths are indicated, the time-durations are specified similarly (plots are generated using oversampling).

for unlicensed operations in the U.S. television broadcast bands. Finally, as a kind of theoretical lower limit on spectral leakage we use the -100dBc point.

Fives signals S_{TFL} of degree 1..5 are shown in figure 4.1 on a logarithmic scale whereby the 0dBc, -60dBc and -100dBc bandwidths are indicated. The figures illustrate the fast exponential decay of the signals over time and frequency. Note that different dBc definitions for bandwidth- and time-durations may be used, e.g. -60dBc definition for the symbol bandwidth and -40dBc for the symbol time-duration. Despite this comment, this thesis applies equal dBc definitions for specifying the bandwidth and time-durations of symbols.
The occupied time durations and bandwidths for signals S up to degree 42 are plotted in figure 4.2 for 0dBc, -60 dBc and -100dBc. Although the absolute symbol durations and symbol bandwidths increase per added carrier, the increase per carrier becomes smaller and smaller.

The time-bandwidth products are calculated by multiplying the symbol time-duration and symbol bandwidth (for the different dBc definitions). This results in almost straight lines, indicating a linear dependence of the time-bandwidth product on the number of carriers in the signal set S_{TFL}. It is known that the maximum number of degrees of freedom per time-bandwidth is (asymptotically) given by $2T_s BW_s$ with T_s the symbol time and BW_s the symbol bandwidth [11]. These degrees of freedom are relevant as they indicate the number of degrees which can be modulated. It can be seen in figure 4.3 that the signals S_{TFL} with their 0dB points quite closely approximate this line. The -60dBc and -100dBc time-duration and bandwidth definitions are associated with larger time-bandwidth products, because part of the exponential tail is now taken into account. For comparison, time-bandwidth products are

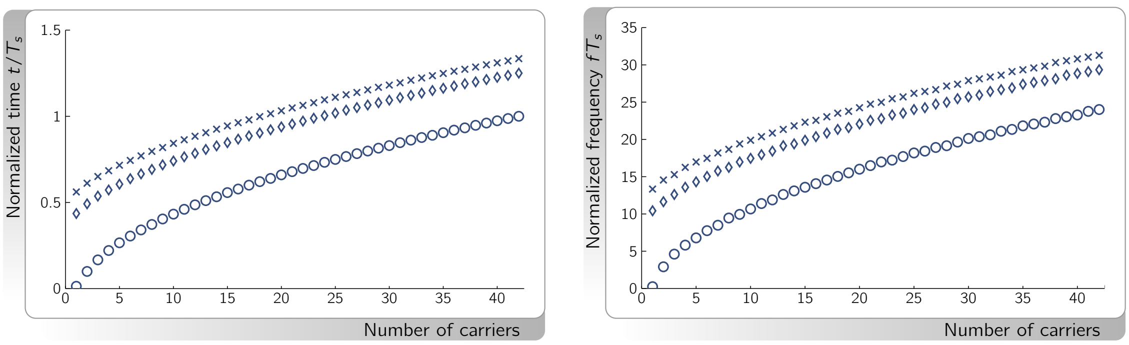

Figure 4.2 | The time duration and bandwidth for signals S_{TFL} with duration and bandwidth specified for the last local maxima before the exponential tail 0dBc (o), the -60dBc ($\diamond$) and -100dBc (x) points in time and frequency.

plotted for raised cosine filters with different roll-off factors. Raised cosine filters are characterized by the roll-off factor which is a measure for the smooth roll-off of the signals as well as extension of the symbol period (for time-domain pulse-shaping) [62]. High sidelobe suppression is achieved using large roll-off factors at the cost of larger symbol times/bandwidths of up to 100% of the original symbol time/bandwidth. [63] states that roll-offs as large as 1 may be necessary for good sidelobe suppression. Figure 4.3 shows the time-bandwidth product for the 0dBc definitions for multiple carriers. In addition, the sidelobe suppression using raised cosine filters for different roll-off factors are given.

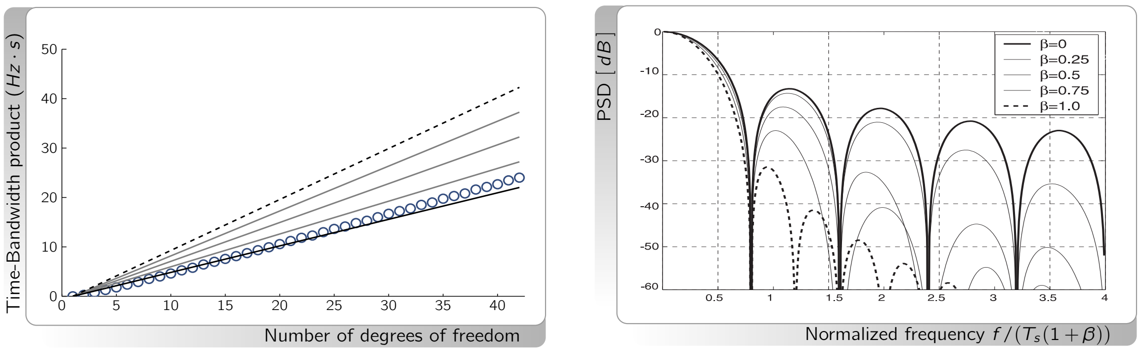

Figure 4.3 | Time-bandwidth products for multi-carrier communication using the signal set S_{TFL}. The time-bandwidth product is specified for the last local maxima before the exponential tail 0dBc (o) in time (power) and frequency (PSD). The solid black line represents the theoretical minimum time-bandwidth product per carrier of 1/2. The dashed black line represents the time-bandwidth product corresponding to a raised cosine roll-off β of 1. Similarly the time-bandwidth products for other roll-off factors are plotted (left) together with achievable sidelobe suppressions (right, source: [62]). Note that the solid black line represents unfiltered / conventional OFDM.

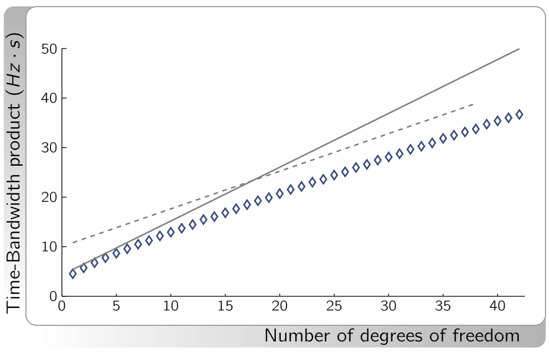

Figure 4.4 | Time-bandwidth products for multi-carrier communication using the signal set S_{TFL}. The time-bandwidth product is specified for the -60dB ($\diamond$) points in time (power) and frequency (PSD). The solid gray line represents the time-bandwidth products for the raised cosine filter with roll-off 1. The dashed gray line shows the time-bandwidth products corresponding to a roll-off factor of 0.5. Lower roll-off factors are not plotted, but have a considerable higher time-bandwidth product for a small number of carriers. Based on figures from [62].

In recent years Hermite functions have also been mentioned in connection with pulse-shaping filters. Haas and Belfiore were in 1994, to the knowledge of the author, the first to use the Hermite functions as a pulse-shaping prototype filter for multi-carrier communication [53]. In 2005 Kurt e.a. claimed that the Hermite pulse-shaping filter is better localized than the often mentioned Gaussian Isotropic Orthogonal Transform Algorithm (IOTA) prototype pulse-shaping filter [64]. This is in accordance with our findings in chapter 2. A recent overview article of Farhang-Boroujeny and Yuen regarding filterbank multi-carrier systems also mentions the superior localization properties of the Hermite pulseshaping filter [65]. In general sidelobe suppression, achieved by pulseshaping filters, comes at the price of excess time-durations and/or excess bandwidths. Using OFDM-OQAM, it is claimed that these excess time-durations and/or excess bandwidths can be limited by separating the I & Q components and transmit filtering each path separately [65] and [66], although Beaulieu points out some problems regarding equalization with this approach [34].

Figure 4.3 shows that the signals S_{TFL} have a time-frequency product per degree of freedom close to the theoretical maximum of $2T_sBW_s$. It is close but not exact. The correspondence theory, a theory underlying quantum mechanics posed by Niels Bohr, states that the new quantum harmonic oscillator model should be in support of the (old) classical harmonic oscillator model [67]. The classical model is built upon (damped) harmonic/sinusoidal signals while the quantum harmonic oscillator is modeled using Hermite functions. In accordance with the correspondence theory, we observe that the behavior of high degree Hermite functions converges more and more to classical harmonic signals. Hence, we pose the expectation that the Hermite signals similar to the sinusoidal signals approach the theoretical limit of 2 degrees of freedom per T_sBW_s when the signals sets increase and are well-designed. Next section gives the explanation for the difference between this expectation and figure 4.3.

The offset in time-frequency product for -60dBc and -100dBc is explained by the time- and frequency space necessary for the exponential tails to decay. As the 0dBc definition does not account for the exponential tail, the time-frequency product for one carrier is (theoretically) 0. We observe that the signals S_{TFL} are not only localized (defined by variances), but also have a small time-bandwidth product indicating high data-throughput. For small carrier sets the -60dBc time-bandwidth product is similar to the product for a raised cosine filter with roll-off 1. For larger carrier sets, the time-bandwidth product becomes smaller and more similar to the 0.5 roll-off. Although smaller roll-offs more closely approximate the lower bound of $2T_sBW_s$, the time-bandwidth product for -60dBc is quite large. This is caused by the slow decay of the shaped spectrum. For a roll-off of 0 we have the sinc-pattern associated with conventional OFDM, which leads to a very large -60dBc time-bandwidth product.

4.4 Multi-user application

Achievable datarates are directly related to the bandwidth, power and noise as set out by the Shannon limit. We make the distinction between datarates achievable in a single-user case, i.e. with no notice of other spectral users, and in a real-world multi-user case. In the multi-user case, the spectral leakage of one user is likely to limit the achievable datarates for another user. The network throughput C_n (in bits/s), the sum of all the link capacities of individual users, can be defined as:

$$C_n = \sum_{u=1}^{U} C_u \tag{4.1}$$

whereby U is the number of total users and each user achieves an individual user datarate of C_u (bit/s). In a multi-user, spectrum-scarce environment, the goal is no longer to optimize C_u, but to optimize the network throughput C_n. A special variant of OFDM, OFDMA allocates certain subcarrier sets (out of a larger set) to different (synchronized) users in order to come to a better network utilization, i.e. to increase C_n. Instead, wireless devices employing OFDM are usually not synchronized and their spectral leakage leads to mutual interference and significantly lower the network throughput.

The signals S_{TFL} are localized in time and frequency. Despite their good localization properties the functions actually extend over the domains $[-\infty, \infty]$ both in time and frequency. Using the time-duration and bandwidth definitions, of -60dBc or -100dBc multi-user communication without noticeable interference can be established. As the signal set S_{TFL} is based on Hermite functions, which are the eigenfunctions of the FrFT, the functions S_{TFL} have their power isotropically spread over time and frequency. For the isotropic case, the time-frequency lattice supporting 16 spectral users is sketched in figure 4.5I. Time- and frequency dispersion as a consequence of multi-path effects and Doppler shifts lead to ISI and ICI respectively. The effects of ISI and ICI may be limited by scaling the signals S_{TFL} in time and frequency according to the time- and frequency dispersion $\Delta t/\Delta f$. This suggestion has also been made

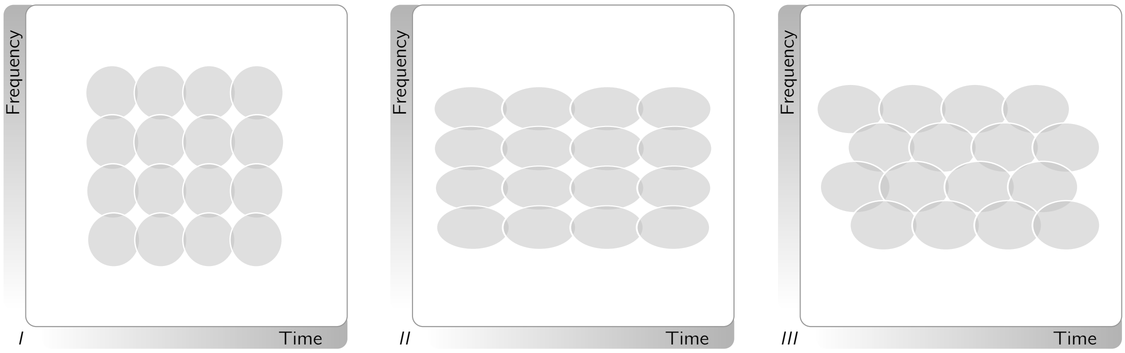

Figure 4.5 | *I*. Regular grid of isotropic time-frequency distributed signals S_{TFL}. *II*. Regular grid of time-frequency scaled signals S_{TFL} according to time- and frequency dispersion. *III*. Grid with time-frequency scaled signals S_{TFL} with time shift of $1/2T_s$ for odd rows.

and discussed by Strohmer and Beaver [68]. Such a scaling is schematically shown in figure 4.5 II.

It may be understood from figure 4.5 I&II that the allocated time-frequency spaces are not optimally packed. A better allocation is obtained when the time-frequency spaces are spaced by $1/2T_s$ for adjacent frequency bands such that the sphere-packing of figure 4.5III is obtained.

We arrive at the explanation for the fact that the signals S_{TFL} did deviate from the Shannon maximum of $2T_sBW_s$ in figure 4.3. Namely, the time-bandwidth products for different dBc definitions were calculated by a simple multiplication of T_s with BW_s. But, both the discussion of the Hermite functions as eigenfunctions of the Fourier Transform / FrFT as well as the Gaussian pulse of figure 2.7 lead us to the conclusion that the energy is distributed isotropically over the time-frequency lattice. Accordingly the time-frequency lattice surrounded by the dBc definition is not a square, but a circle. The area, assuming $T_s = BW_s$, is a circle with time-frequency area πT_s^2 rather than $4T_s$. This gives a difference of $4/\pi \approx 1.27$ and explains the deviation of the Shannon limit encountered in the last section. Compensating the results of figure 4.3 leads to the conclusion that the signals S_{TFL} contain a number of modulation degrees of freedom, equal to $2T_sBW_s$. Accounting for the exponential tail, e.g. by the -60dBc definition, leads to a slightly larger time-bandwidth product compared to the 0dBc definition.

Two important conclusions can be drawn:
◇ 1. For the 0dBc (≈ pass-band) time and bandwidth definition the signals S_{TFL} lead to approximately 2 degrees of modulation freedom per unit time-frequency area, which is the theoretical optimum.
◇ 2. For any other dBc definition of time and bandwidth, the occupied time-frequency area per degree of freedom for signals S_{TFL} is approximately the optimum achievable for that dBc definition.

The first statement has been discussed above. The second statement is motivated by the first statement and the fact that the tail is exponential and there is no function decreasing faster both in time and in frequency (chapter 2). So if statement 1 is true then, accounting for the exponential tail, also statement 2 holds. The first statement is especially relevant in the single-user case. Note that there is no difference with conventional OFDM and both have the same dimensionality per unit time-frequency area. The exception is formed by the cyclic prefix, which increases the time-bandwidth product of conventional OFDM. The second statement is particularly relevant for multi-user settings as the signals S_{TFL} do not only achieve high single-user datarates, but thanks to their good localization, enable also a high network throughput.

4.5 Performance in mobile radio channels

The elementary part of radio communication is the physical propagation of electromagnetic radiowaves through some medium. Instead of dealing with the physics involved with propagating electromagnetic waves, we stick to common models for the mobile radio channel. This section discusses and tests the signals S_{TFL} in comparison with OFDM signals for two general channel models, the AWGN and Rayleigh fading channel.

4.5.1 Additive White Gaussian Noise channels

In an AWGN channel, signals are degraded by added noise. The AWGN model assumes that the noise has a Gaussian amplitude distribution, its autocorrelation is a delta-function and the PSD is constant/white, whereby the noise variance is related to the PSD noise level. BER expressions for antipodal/BPSK schemes can be found in standard textbooks, although they are more elaborate for larger constellations. An approximate expression for the BER in AWGN for Amplitude Shift Keying (ASK)/PAM modulation schemes with M constellation points is given by [69]:

$$P_b \approx \frac{2(M-1)}{kM} \cdot Q\left(\sqrt{\frac{6k}{M^2-1}\frac{E_b}{N_0}}\right) \text{ with } k = \log_2(M) \tag{4.2}$$

The constellation points are located at $-(M-1), \cdots, -3, -1, 1, 3, \cdots, (M-1)$ with every constellation point normalized by $1/\sqrt{E}$ with E representing the average 'energy' of the M constellation points.

The transmission and reception of the signals S_{TFL} and conventional OFDM signals has been simulated according to the setup described in section 4.2. The signal $\text{rx}(t)$ equals $\text{tx}(t) + n(t)$, whereby $n(t)$ is AWGN. The simulated and theoretical BERs for different Effective energy per bit to noise PSD ratios (EbN0s), are shown in figure 4.6. The theoretical lines correspond to equation 4.2. The simulations of OFDM signals and signals S_{TFL} show similar BERs. As discussed in chapter 3, the signals should be orthogonal and interpreted by correlators/matched filters in order to be optimal in AWGN. As both OFDM and the signals S_{TFL}, and the simulation setup, fulfill these requirements, it makes sense that both signal sets match the theoretical BERs given by equation 4.2.

4.5.2 Fading channels

Although AWGN may be an adequate model when receiver and transmitter find themselves at a stationary position in the open field, in practice obstacles and movements of objects cause significant signal impairments. A more comprehensive radio channel model also accounts for fading. Among the types of fading a distinction can be made between large scale fading and small scale fading [70]. Large scale

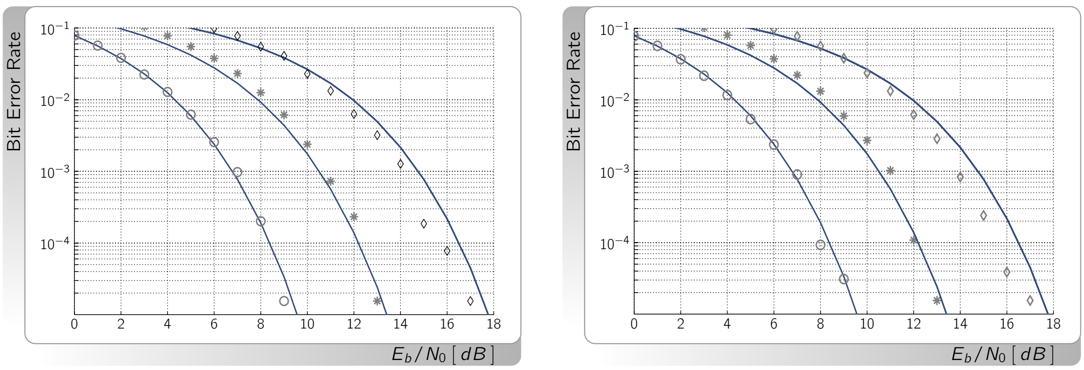

Figure 4.6 | Theoretical and simulated Bit Error Rates for OFDM (left) and proposed signal set S_{TFL} (right). Signals are degraded by AWGN and signals are modulated according to BPSK (o), 4PAM ($*$) and 8PAM ($\diamond$) modulation schemes. Note, the $EbN0$ for OFDM does not take the energy spent for the cyclic prefix into account.

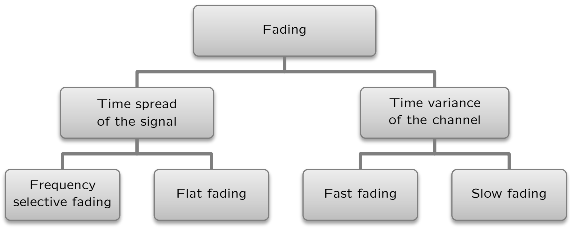

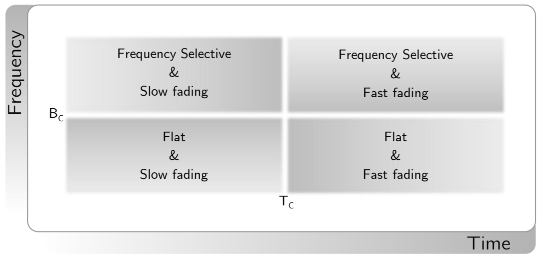

Figure 4.7 | Overview of different forms of small-scale fading (left) and the different types of signal fading as a function of signal duration and signal bandwidth (right).

fading is caused by signal variations due to the position of transmitter, receiver and obstacles and is a slowly varying process. The received signal power equals the transmit power minus the mean path-loss, whereby variations around the mean are usually modeled by a lognormal distribution [70].

In contrast with large-scale fading, small-scale fading is not associated with variations of the mean of the received signal, but rather with instantaneous changes in signal amplitude. Small-scale fading manifests itself by two mechanisms, time-spreading of the signal and time-variant behavior of the channel [70]. For time-spread of the signal, a distinction can be made between frequency-selective and flat fading. For the time-variant behavior of the channel we have on one hand channel variations which are relatively constant over a single symbol time, slow fading, and on the other hand channel variations which manifest itself during a symbol time, fast fading. Figure 4.7 gives an overview of the different types of small-scale fading. Two important characteristics for fading are the coherence time and the coherence bandwidth. Multi-path reflections can cause considerable differences in ray propagation times. These time delays give for different frequencies different phase shifts. The coherence bandwidth B_c is an indicator for the bandwidth for which the phase shifts can be assumed equal. If the signal bandwidth B_s is smaller than the coherence bandwidth B_c, we speak of flat fading while in the case $B_s > B_c$ the fades are frequency dependent, i.e. frequency selective. The coherence time T_c indicates the time for which the channel response is relatively constant. If the symbol time T_s is larger than the coherence time T_c, then the fading is referred to as fast. On the other hand when $T_s < T_c$, one speaks of slow fading. A schematic overview of these four conditions is given in figure 4.7.

The simulations are based upon a common assumption of slow, frequency selective fading. The exhibit discusses this type of fading.

◇ **Rayleigh fading**

In real-world communication, it is likely that several rays propagate through the air along different paths. The rays add up to the received signal rx(t). Under the assumption that there is no Line-of-Sight (LOS) component, the received signal can be modeled as:

$$\mathrm{rx}(t) = \sum_{i=1}^{R} \gamma_i \cos(\omega_s t + \phi_i) \tag{4.3}$$

whereby R is the number of reflective rays from transmitter to receiver and ω_s the center frequency of the transmitted signal. ϕ_i represents the phase change caused by a differences in relative path lengths and is assumed to have a uniform distribution over $[0, 2\pi]$ while the amplitude of the ray γ_i is generally assumed to vary according to a normal distribution. When there is motion of transmitter, receiver or reflective objects, Doppler shifts need to be taken into account. We follow the approach as given by [71].

The Doppler shift, the relative change in frequency, is given by:

$$\omega_{d_i} = \frac{\omega_s \cdot v}{c} \cos(\psi_i) \tag{4.4}$$

whereby ψ_i represents the angle of motion of the ray relative to the receiver and is assumed to be uniformly distributed over $[0, 2\pi]$. The variable v resembles the speed of the moving object and c represents the speed of light.
Accounting for the Doppler shift, the received signal $\mathrm{rx}(t)$ becomes:

$$\mathrm{rx}(t) = \sum_{i=1}^{R} \gamma_i \cos(\omega_s t + \omega_{d_i} t + \phi_i) \tag{4.5}$$

The signal can be rewritten as a sum of an in-phase (I) and a quadrature (Q) component [71]:

$$\mathrm{rx}(t) = I(t)\cos(\omega_s t) - Q(t)\sin(\omega_s t) \quad \text{with} \quad \begin{aligned} I(t) &= \textstyle\sum_{i=0}^{R-1} \gamma_i \cos(\omega_{d_i} t + \phi_i) \\ Q(t) &= \textstyle\sum_{i=0}^{R-1} \gamma_i \sin(\omega_{d_i} t + \phi_i) \end{aligned} \tag{4.6}$$

For large values of R, i.e. a large number of independent identically distributed rays, the in-phase and quadrature components are Gaussian shaped [71]. The sum of zero-mean squared independent Gaussian random variables has a Chi-square distribution. For the squared Gaussian I and Q components of equation 4.6, under assumption of equal variance, we speak of a chi-square probability distribution with two degrees of freedom. The PDF corresponding to the envelope $\sqrt{I(t)^2 + Q(t)^2}$ is then said to Rayleigh distributed. The PDF of a Rayleigh distribution is [61]:

$$p(z) = \frac{1}{2\sigma^2} e^{-\frac{z}{2\sigma^2}} \text{ for } z \geq 0 \tag{4.7}$$

whereby σ^2 is the variance of the Gaussian shaped I and Q components, being equal. Note that the summed amplitude of the received signals/rays is distributed normally. This implies that there is no dominant LOS component. If there is a dominant contribution of one component (typically LOS) then the envelope is better described by the Rice distribution, but this is outside the scope of this research.

Two models have been used to simulate Rayleigh fading. First, a large set of independent rays (undergoing a Doppler shift) has been modeled to simulate fading. Second, normally distributed I and Q components (as explained in the exhibit) are used as an approximate model of fading. Both models lead to the same results as long as the number of rays is large enough, path delays are shorter than the cyclic prefix (in case of OFDM), path delays are large enough to have uniformly distributed phase shifts over $[0, 2\pi]$ and under the assumption that channel estimation and equalization is perfect in both models. The signals S_{TFL} do not need a cyclic prefix as the signals are smooth over time and a shift in time leads to a fraction of the ISI compared to OFDM signals.

The BERs for the signals S_{TFL} and OFDM signals in a Rayleigh fading channel are shown in figure 4.8. The theoretical BERs are obtained by MathWorks Matlab Communication toolbox using the command *berfading* for PAM. As the expressions are quite elaborate, they are not listed here. Refer for more information to the Matlab documentation or to the mathematical background [72].

We encounter differences for the signals S_{TFL} versus the OFDM signals in robustness against fading. The OFDM signals perform better for low E_b/N_0 while the signals S_{TFL} seem to perform better for high E_b/N_0. The underlying reason may be that the signals S_{TFL} occupy larger bandwidth (on average) than OFDM signals. If there is a relative strong frequency selective fade, all signals S_{TFL} are affected while only a couple OFDM subcarriers are impacted. When the disturbance is smaller, the 'wide-band' signals S_{TFL} are robust against the fades, while the fades still affect the small-band OFDM signals. The number of bits used in simulation were limited to 10^5, so no real conclusions can be drawn for low BERs. In case the channel impulse response is larger than the cyclic prefix for OFDM signals, then the BERs related to OFDM are severely degraded and the signals S_{TFL} perform significantly better thanks to their time-frequency localization property. In addition, the EbN0 for OFDM does not account for the energy spent in the cyclic prefix, so the effective energy per bit is in practice larger.

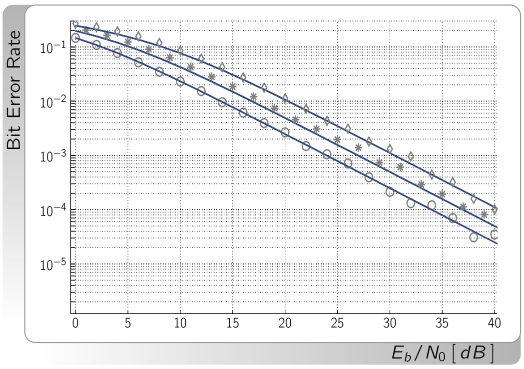

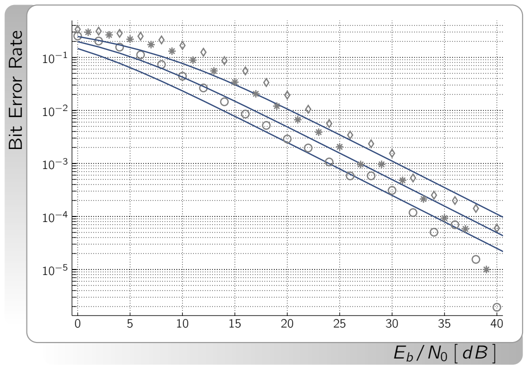

Figure 4.8 | Simulated Bit Error Rates for OFDM (left) and proposed signal set S_{TFL} (right). Signals undergo Rayleigh fading in an AWGN channel. Theoretical lines according to [72]. Applied modulation schemes are BPSK (∘), 4PAM (∗) and 8PAM (⋄). Plots were generated using $> 10^5$ bits. No conclusions can be drawn based on BERs lower than 10^{-4}. Note, the EbN0 for OFDM does not take the energy spent for the cyclic prefix into account.

4.6 Peak to Average Power Ratio

Chapter 3 discussed the crest factor/PAPR as a criterium for the basis set of communication signals. As the PAPR is competing with entropy of the transmit signals, the PAPR was excluded from the signal criteria. Nevertheless, from a system perspective, the PAPR is quite important. It directly imposes requirements on the dynamic range of both transmitter and receiver building blocks. Section 3.4 stated that a Gaussian distribution of the random amplitude of the transmit signal at a distinct moment in time, without limit on the peak power, is optimal to achieve maximum entropy. Independent, identical uniformly distributed random variables tend, for large sets, to a Gaussian distribution according to the central limit theorem. When dealing with both in-phase and quadrature components, we have two times a Gaussian distributed random variable. Therefore, the probability distribution of the summed random power of the in-phase and quadrature components is a chi-square distribution with two degrees of freedom (as explained in section 4.5.2). The envelope of the transmit signal is then given by the square root of the summed powers, leading to the Rayleigh distribution. Concluding, in case of maximum entropy for both an I & Q component, the instantaneous power at a certain sampling time is expected to be a Rayleigh distributed random variable.

Simulations have been carried out for BPSK using 108000 bits simulating the PAPR both for OFDM signals and signals S_{TFL}. The PAPR is not a meaningfull measure as the probability for the absolute peak to occur, for multi-carrier communication with a large numbers of carriers, tends to zero. The PDF and complementary Cumulative Density Function (CDF) of the PAPR are more meaningful and are plotted in figure 4.9. The histogram reveals a PDF similar to the Rayleigh distribution. Evaluation of the complementary CDF gives a chance of 0.1% for a PAPRs of 6.2 (or in decibels 7.9dB).
To assist a fair comparison of the results it is recommended to carry out comparisons with known expressions of the PAPR for OFDM signals. A good overview of PAPRs for OFDM is presented by Ochiai [73]. Based on the simulation results, the PAPR for the signal set S_{TFL} seems to be equal to the PAPR for OFDM. As stated before, the Rayleigh distributed PAPRs may imply that the transmit signals approach the theoretical maximum of entropy at the price of a high PAPR. If no measures are taken, the power peaks may lead to clipping and/or saturation of analog transceiver blocks. This leads to signal distortion, which in turn causes spectral leakage. Measures need to be taken - at the cost of achievable datarate - to prevent or reduce these power peaks. These steps are preferably taken while designing a set of signals (when it is known to be a limitation beforehand). In case the PAPR needs to be reduced at run-time, PAPR reduction techniques used for OFDM can be applied to S_{TFL} as well. A good overview of PAPR reduction techniques is presented by [74] and [75].

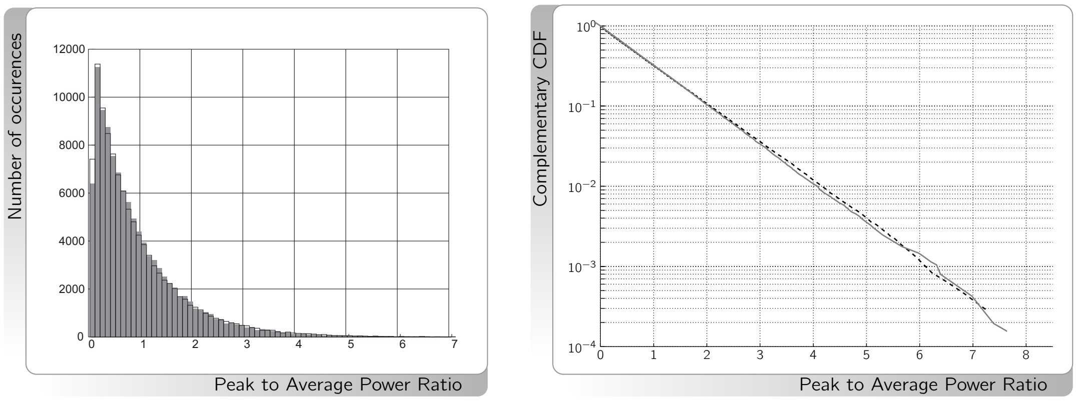

Figure 4.9 | Histogram of Peak to Average Power Ratio occurences both for OFDM (solid/gray) and signals S_{TFL} (black line) at the left side. The PAPR seems to be Rayleigh distributed. Right figure gives the cumulative Probability Density Functions for OFDM (solid/gray) and signals S_{TFL} (black, dashed line).

4.7 Consequences for hardware

4.7.1 Transmitter

OFDM got a serious chance after the notice of using the inverse and forward Discrete Fourier Transform for the generation and interpretation of OFDM waveforms. The computational complexity was proportional to N^2 for the DFT realizations while the fast Fourier transforms reduced this to $N \log_2(N)$. The generation and evaluation of Hermite functions is not enhanced by the Fourier transform as the functions occupy several frequency bins. Some attention has been paid to the implementation of a Hermite transform, i.e. an operator mapping a signal in a space R^N to N basis Hermite functions (or signals like S_{TFL}). Leibon e.a. have investigated fast algorithms for the approximation of Hermite functions (to analyze protein structures) and made a first start in the development of fast Hermite transforms with complexity proportional to $N \log_2(N)$ [52]. Evaluation and elaborating on such a transform may enhance generation and evaluation of the signals S_{TFL}.

Without a fast Hermite transform, we propose to store the basis signals S_{TFL} in a local memory. Signal sets S_{TFL} with signals modulated up to degree 64, under the assumption of 16bit quantization and 8, 16, 64 constellation points require memories sizes of 64, 128 and 512 kilobytes respectively. The transmit signal can be obtained by adding the waveforms with a total of $N(N-1)$ additions. When $N = 64$ this gives about 4000 additions. Evidently, one can also carry out the modulations by N^2 multiplications and using a memory of 8kilobytes.

The new signal set S_{TFL} is designed to limit spectral leakage. There are two additional causes of spectral leakage. First, non-linearities in analog transceiver blocks can cause intermodulation products which are likely to fall out-of-band and contain significant power. Knowing the transmit signal as well as the non-linearity of the transmitter, the signal can be pre-distorted to compensate the intermodulation products. Second, the transmit signals based on the modulated signals S_{TFL} have a high PAPR. Saturation of amplifying elements and/or clipping of the signals leads to distortion, causing significant out-of-band power. To prevent clipping, measures should be taken to increase the dynamic range of the whole transceiver system. This comes at the price of a high inefficiency of the power amplifier. Another option is to combat the peak powers by PAPR reduction techniques [74] and [75].

To overcome spectral leakage associated with conventional OFDM signals the transmit signal is usually shaped by time-domain pulse-shaping. Such transmit filters tend to become quite long and complex in order to achieve good sidelobe suppression. Instead, the signals S_{TFL} immediately fulfill the criterium of time-frequency localization and do not require filtering. The abrupt phase and amplitude changes

associated with conventional OFDM also cause problems, as these signals are not realizable and the high frequency components are likely to be filtered out after they leave the DAC. This leads to distortion in the transmitter and degrades the achieved BERs. S_{TFL} as well as OFDM signals which are pulse-shaped, are more localized in frequency and do not have this problem.
Revisiting chapter 3, two major problems with Hermite functions were identified. The non-uniform sampling of Hermite functions as well as the DC components in the even order Hermite functions. The signals S_{TFL} overcome these problems. They are uniformly sampled and all signals are zero-mean, which enhances actual implementation.

4.7.2 Receiver

Correlation demodulators are known to be optimal receivers for AWGN [61]. Instead of performing cross-correlations and evaluating the output once per symbol period, an identical operation can be performed by matched filters with lower computational complexity. Matched filters are similar to the DFT and involve N^2 multiplications and $N(N-1)$ additions. The 'correlation' between received signal $\mathrm{rx}(t)$ and the signals S_{TFL} is calculated using real operations. This in contrast with OFDM where the FFT involves $N \log_2(N)$ complex additions and $N/2 \log_2(N)$ complex multiplications. Instead of generating the signals S_{TFL} it is proposed to save the basis waveforms in a small memory (similar to the transmitter, one memory can be used for both transmitter and receiver). For a correct correlation of the received signal timing synchronization is very important. The zero-mean property of the signals S_{TFL} may facilitate synchronization, although more research is recommended.

To be robust in fading channels, channel estimation and equalization are necessary. In case of conventional OFDM, the subcarrier spacing is such that each carrier bandwidth is smaller than the coherence bandwidth (as discussed in section 4.5.2). As a result, equalization reduces to one complex multiplication per subcarrier. Because the signals S_{TFL} use a wider bandwidth, equalization becomes more complex. Equalization is applied in numerous transmission systems and is well treated by standard textbooks like [61] and [24]. Channel estimation, using pilot symbols, can be done independent from the type of signals transmitted or received and no differences in complexity are expected for OFDM signals versus the signals S_{TFL}.

One of the drawbacks of OFDM is its sensitivity to frequency offsets and phase noise leading to ICI. Although not taken into account as a signal design criterium, the sensitivity of signals S_{TFL} for frequency offsets and phase noise may have a large impact on the oscillator requirements. Namely the power necessary for the oscillator is directly related to the amount phase noise introduced. It is recommended to explore ICI for transceivers employing signals S_{TFL} for different situations and mainly in comparison to OFDM.

It is recommended to adopt quadrature modulation. This leads to the modulation of both an in-phase (I) and a quadrature (Q) set of Hermite signals. Exploration of efficient ways to implement quadrature modulation is recommended.

4.8 Discussion of the results

Concluding, six performance measures have been formulated targeting the effectiveness and efficiency of a transmission system employing signals S_{TFL}. The measures target the datarates, multi-user communication, BERs in different channels, the PAPR and the hardware complexity of transmitter and receiver. The datarates in the single-user case are similar to OFDM while differences are encountered multi-user cases. Where the bandwidth products for OFDM using the -60dBc definition would require guard bands of hundreds of carriers, the bandwidth only slightly increases for the signals S_{TFL}, thanks to their exponential decrease over time- and frequency. In order to come to an optimum number of carriers per time-bandwidth product, attention should be paid to the effective assignment of time- and frequency space to several users.

The BERs have been simulated for AWGN and fading channels. The results for AWGN channels are the same for OFDM and signals S_{TFL}, except for the energy spent for a cyclic prefix in case of OFDM. For fading environments, in case we deal with low $EbN0$, the BERs are relatively high for signals S_{TFL} compared to OFDM signals. For lower BERs the performance of signals S_{TFL} is approaching or even better than OFDM. For the point of interest (around a BER of 10^{-3}) there is no difference in BER performance between OFDM and signals S_{TFL}. It was expected that the signals S_{TFL} would be more immune against frequency selective fading than OFDM due to the fact that the signals on average occupy a wider bandwidth than OFDM signals. It is recommended to perform further analysis on the BERs for signals S_{TFL} in fading channels. In contrast with OFDM signals, no cyclic prefix is necessary for the signals S_{TFL}, saving some energy per bit.

The PAPR for OFDM and quadrature modulated signals S_{TFL}, using BPSK, has been simulated. Based on the simulations, the PAPR for S_{TFL} and OFDM signals turns out to be the same. It is recommended to carry out comparisons with literature to verify the simulation results. As discussed in chapter 3 the high PAPR is the price we need to pay for the entropy of the transmit signals constructed by signals S_{TFL}. To deal with the problem of PAPR, similar techniques can be used as in OFDM. Finally, the complexity of transceivers employing signals S_{TFL} has been discussed. The digital complexity for generating OFDM signals is proportional to $N \log_2 N$ complex additions and multiplications. For the signals S_{TFL} the generation involves $N(N-1)$ real additions and a memory for saving the basis waveforms. The receiver can use the same memory while using N^2 real multiplications for the matched filter operations. As stated in the previous section, for quadrature modulation we deal with both I and Q components, leading to an increase in computational complexity by a factor 2.

CHAPTER 5

Conclusions

5.1 Research aim & findings

The ever increasing usage of the radio-spectrum raises questions regarding the usage of Orthogonal Frequency Division Multiplexing. OFDM is generally regarded as the primary multi-carrier modulation technique, but devices employing OFDM suffer from spectral leakage. Spectral leakage may cause interference to other wireless devices, leading to higher Bit Error Rates (BERs), retransmissions and ultimately congestion of the wireless channel. Conventional solutions to deal with the problem of spectral leakage include guard spaces, active interference cancellation, cancellation carriers, carrier weighting, constellation mappings and pulse-shaping. Although successful to smaller or larger extent, these measures generally demand a trade-off between spectral efficiency, achievable datarates, bandwidth, used power and noise performance. The extensive usage of these methods can be debated. The methods deal with the consequences, the OFDM sidelobes, rather than targeting the problems, the basis signals themselves.

This thesis addresses the basis signals for communication. An elaborate treatment in chapter 2 led to Hermite functions as a set of solutions to time-frequency uncertainty. Despite the optimal time-frequency localization property of Hermite functions, that does not necessarily imply that the signals are suitable for communication. Therefore, ten attributes of a basis set of signals have been discussed: continuity, linear dependence, orthogonality, correlation, energy, entropy, crest factor, localization, timing and frequency sensitivity. These attributes led to the formulation of criteria which have been used to design a set of basis signals S_{TFL} for communication. In contrast with Hermite functions, the signals S_{TFL} are discrete, limited in time and frequency, zero-mean and uncorrelated.

In order to assess the suitability of the signals S_{TFL} for communication, a number of performance measures have been defined targeting the effectiveness and efficiency of communication. While the effectiveness addresses the achievable datarates under different circumstances, the efficiency covers the power efficiency and hardware complexity of transceivers employing signals S_{TFL}. The datarates in single-user case are similar to OFDM while differences are encountered for practical multi-user environments. Where the bandwidth definition of -60dBc (to conform to U.S. FCC regulations) would require guard bands of hundreds of carriers for conventional OFDM and still significant for raised cosine filtered OFDM signals, the -60dBc bandwidth for signals S_{TFL} is only slightly higher than the pass-band bandwidth. It is shown that the signals S_{TFL} are near-optimal performing in single-user case, and thanks to their exponential decay in time- and frequency, also perform near-optimal in multi-user environments. The Effective energy per bit to noise PSD ratio (EbN0) for Additive White Gaussian Noise (AWGN) and fading channels is approximately equal for signals S_{TFL} and OFDM signals (evaluated at BER $\approx 0.1\%$). The EbN0 is slightly higher for conventional OFDM signals compared to signals S_{TFL} due to the necessity of a cyclic prefix.

As the Peak to Average Power Ratio (PAPR) trades off with entropy, no PAPR restraint has been set for the design of signals S_{TFL}. The PAPR is equal for the signals S_{TFL} and the OFDM signals. As long as there is no 'fast Hermite transform' the digital complexity of generation and interpretation of signals S_{TFL} is proportional to N^2 rather than $N \log_2(N)$ for OFDM, with N the number of carriers and sampling points. It is proposed to store the basis signals S_{TFL} in a memory (in kilobyte range). To construct a transmit signal employing the signals S_{TFL}, $N(N-1)$ real additions are required. The receiver can be built up by N matched filters involving approximately N^2 real multiplications and additions in total. Compared to Hermite functions, the signals S_{TFL} are better suited for implementation, as the signals are uniformly sampled and lack a DC component.

To recapitulate, the aim of this research has been formulated as reducing spectral leakage while maximizing the effective data transfer rate and staying within energy, bandwidth and complexity budgets. We have been able to reduce spectral leakage by using signals optimally localized in time- and frequency such that the communication of one user leads to minimum interference to other users. Regarding the achievable data-rates it was discussed that for any dBc definition used to define the symbol time and duration, the datarates employing signals S_{TFL} are (theoretically) equal or higher than for OFDM given a certain bandwidth. While energy per bit is expected to be equal or a bit lower, thanks to the fact that no cyclic prefix is necessary, the hardware complexity increases slightly.

A short list of the main topics brought up in this thesis are:
◇ Overview and critical discussion of conventional methods to combat spectral leakage
◇ Analysis of time-frequency uncertainty in relation to communication signals
◇ Investigation of the delta Dirac function in relation to Hermite functions
◇ Discussion of power limited versus energy limited signals in relation to entropy and PAPR
◇ Formulation of criteria for a basis set of signals for communication
◇ Design of a set of signals S_{TFL} based on Hermite functions and adapted to meet design criteria
◇ Discussion on the usage of the Shannon limit for datarate analysis
◇ Performance evaluation of a communication system employing signals S_{TFL}.

5.2 Limitations & Discussion

As this thesis addresses a wide variety of topics concerning communication, some discussions are of limited length. Subjects like sampling, entropy and sphere-packing were briefly discussed while matters like I & Q mixing, synchronization, channel estimation and equalization have only been mentioned. Similarly the treatments of fundamental topics like the uncertainty principle, entropy versus PAPR, the application of the Shannon limit and the delta Dirac function are quite compact. The aim has been to cover all considerations relevant for the design and implementation of the signals S_{TFL} rather than giving an elaborate treatment on just a few topics. A limitation of this research is that the sensitivity for time- and frequency deviations was not taken into account while designing the signals S_{TFL}. It is acknowledged that the susceptibility of the signals S_{TFL} for timing and frequency deviations should be limited. This is crucial to combat Inter-Symbol Interference (ISI) and Inter-Carrier Interference (ICI).

The signals S_{TFL} have been compared with conventional OFDM signals. Two remarks can be placed regarding this approach. First, OFDM signals are time-limited while signals S_{TFL} are unbounded over time and frequency, which poses difficulties for comparing the two signal bases. Second, conventional OFDM may not be the best comparison in terms of performance. Filter bank multi-carrier communication achieves a better localization and omits the necessity of a cyclic prefix. Although this thesis addresses spectral leakage related to OFDM, also single carrier modulation techniques suffer from spectral leakage. So, part of the results may be generalized to the larger class of wireless transceiver systems employing sinusoidal signals.

In order to make the Hermite functions feasible for transceivers, the Hermite functions have been modified to the signals S_{TFL}. Regarding the presented performance results, it is important to note that the results have been obtained by conventional methods. No coding, no staggered I & Q paths, oversampling or other implementation tricks have been applied. Such refinements can be applied in future work and may boost the results. Taking into account the spectrum scarcity in these days, as well as a predicted 66x increase in data usage in just four years, there is good evidence to believe that the Hermite functions and their counterparts S_{TFL} can play a major role in communication. The quantum harmonic oscillator model is built upon Hermite functions and is regarded as the improved model of the classical harmonic oscillator model [67]. We like to start the discussion whether Hermite functions constitute an improved model for communication over the conventional sinusoidal base.

5.3 Recommendations for future research

Although numerous questions have been addressed, some questions regarding the signals S_{TFL} are still open. Are larger sets of signals S_{TFL} preferred over smaller sets of S_{TFL} and what are the trade-offs? What is the optimum sampling scheme for the continuous signals S_{TFL}? May the application of the Fractional Fourier Transform (FrFT) increase the robustness against time- and frequency dispersion of the channel (similar to the suggestion in [76])? All of these questions are recommended for future research.

To obtain efficient multi-user communication, the allocation of time-frequency space to different users, i.e. sphere-packing, should be done efficiently. This research has been limited to the time-frequency space and neglected the space dimension. Questions arise about the optimal signals in space-time-frequency.

The set of signals S_{TFL} has been designed for maximum entropy. This led to dropping a restriction on the PAPR. As the PAPR plays an important role in the power efficiency of transceivers, it is recommended to perform the steps in chapter 3 also for the case where a power restriction is applied. Some hints are already given in section 3.4. It is recommended to revisit the basis signals (in this case S_{TFL}) rather than using the signals S_{TFL} in combination with PAPR reduction techniques.

A number of recommendations are mentioned in previous chapters. The investigation of the delta Dirac function led to a Gaussian function. Investigation of the consistency of this finding with conventional Fourier analysis as well as implications of this finding are recommended. In addition, it has been suggested to write expressions for the data throughput in terms of time- and frequency spreads rather than absolute time durations and (pass-band) bandwidths. This would give a meaningful tool to analyze signals which are not strictly band-limited and may provide insight in achievable datarates in multi-user settings. Finally, the lack of a 'fast Hermite transform' increases the digital complexity necessary for generation and correlation of Hermite functions. It is recommended to work on 'fast' implementations of a Hermite transform. A first proposal to such a fast transform can be found in [52].

To verify the performance of Hermite functions and derived signals S_{TFL}, simulations have been carried out. The simulations assumed a number of (analog) building blocks to be ideal. In order to get better insight in the performance of transceivers employing signals S_{TFL} it is recommended to use more elaborate models introducing more non-idealities. Ultimately, it is recommended to build actual transceivers employing signals S_{TFL} to assess the performance of signals S_{TFL} under various circumstances.

List of Acronyms

ADC	Analog-to-Digital Converter
AIC	Active Interference Cancellation
AM	Amplitude Modulation
ASK	Amplitude Shift Keying
AWGN	Additive White Gaussian Noise
BPSK	Binary Phase Shift Keying
BER	Bit Error Rate
CC	Cancellation Carrier
CDF	Cumulative Density Function
CTFT	Continuous Time Fourier Transform
DAB	Digital Audio Broadcasting
DAC	Digital-to-Analog Converter
DC	Direct Current
DSA	Dynamic Spectrum Access
DVB-T	Digital Video Broadcasting - Terrestrial
DFT	Discrete Fourier Transform
EbN0	Effective energy per bit to noise PSD ratio
FCC	Federal Communications Commission
FDM	Frequency Division Multiplexing
FIR	Finite Impulse Response
FFT	Fast Fourier Transform
FrFT	Fractional Fourier Transform
ICI	Inter-Carrier Interference
IIR	Infinite Impulse Response
IOTA	Isotropic Orthogonal Transform Algorithm
ISI	Inter-Symbol Interference
IEEE	Institute of Electrical and Electronics Engineers
ITU	International Telecommunication Union
LNA	Low Noise Amplifier
LO	Local Oscillator
LOS	Line-of-Sight
MAP	Maximum A Posteriori
OFDM	Orthogonal Frequency Division Multiplexing
OFDMA	Orthogonal Frequency Division Multiple Access
OQAM	Offset Quadrature Amplitude Modulation
PAM	Pulse Amplitude Modulation
PAPR	Peak to Average Power Ratio
PDF	Probability Density Function
PM	Phase Modulation
PSD	Power Spectral Density
QAM	Quadrature Amplitude Modulation
QPSK	Quadrature Phase Shift Keying
SNR	Signal to Noise Ratio
STFT	Short Time Fourier Transform
TDMA	Time Division Multiple Access
UWB	Ultra-Wideband
WiMAX	Worldwide Interoperability for Microwave Access
WLAN	Wireless Local Area Network
WRAN	Wireless Regional Area Network

Bibliography

[1] J. Hayes, "A history of transatlantic cables," *IEEE Communications Magazine*, vol. 46, no. 9, pp. 42–48, 2008.

[2] J. C. Maxwell, "A dynamical theory of the electromagnetic field," *Philosophical Transactions of the Royal Society of London*, vol. 155, pp. 459–512, 1865.

[3] A. G. Bell, "Improvements in telegraphy," U.S. Patent no. 174.465, 1876.

[4] R. W. Chang and R. A. Gibby, "A theoretical study of performance of an orthogonal multiplexing data transmission scheme," *IEEE Transactions on Communication Technology*, vol. 16, no. 4, pp. 529–540, 1968.

[5] B. Saltzberg, "Performance of an efficient parallel data transmission system," *IEEE Transactions on Communication Technology*, vol. 6, no. 6, pp. 805–811, 1967.

[6] J. W. Cooley and J. W. Tukey, "An algorithm for machine calculation of complex Fourier series," *Mathematics of Computation*, vol. 19, no. 90, pp. 297–301, 1965.

[7] M. T. Heideman, D. H. Johnson, and C. S. Burrus, "Gauss and the history of the fast Fourier-transform," *Archive for History of Exact Sciences*, vol. 34, no. 3, pp. 265–277, 1985.

[8] B. Hirosaki, "An orthogonally multiplexed QAM system using the discrete Fourier-transform," *IEEE Transactions on Communications*, vol. 29, no. 7, pp. 982–989, 1981.

[9] FCC, "FCC auction 73," March 20, 2010. Link: http://wireless.fcc.gov (visited 14 June, 2010).

[10] M. Stanley, "The mobile internet report," 2009.

[11] C. E. Shannon, "A mathematical theory of communication," *Bell System Technical Journal*, vol. 27, no. 3, pp. 379–423, 1948.

[12] A. Wyglinski, M. Nekovee, and T. Hou, *Cognitive radio communications and networks : principles and practice*. Amsterdam: Academic, 2010.

[13] I. T. Union, "Method for point-to-area prediction for terrestrial services in the frequency range 30 MHz to 3000 MHz," 2005.

[14] J. Mitola and G. Q. Maguire, "Cognitive radio: Making software radios more personal," *IEEE Personal Communications*, vol. 6, no. 4, pp. 13–18, 1999.

[15] FCC, "Facilitating opportunities for flexible, efficient, and reliable spectrum use employing cognitive radio technologies," 2003.

[16] IEEE 1900.1, "IEEE standard definitions and concepts for dynamic spectrum access: Terminology relating to emerging wireless networks, system functionality, and spectrum management," 2008.

[17] C. R. Stevenson, G. Chouinard, Z. D. Lei, W. D. Hu, S. J. Shellhammer, and W. Caldwell, "IEEE 802.22: The first cognitive radio wireless regional area network standard," *IEEE Communications Magazine*, vol. 47, no. 1, pp. 130–138, 2009.

[18] B. Farhang-Boroujeny and R. Kempter, "Multicarrier communication techniques for spectrum sensing and communication in cognitive radios," *IEEE Communications Magazine*, vol. 46, no. 4, pp. 80–85, 2008.

[19] H. A. Mahmoud, T. Yucek, and H. Arslan, "OFDM for cognitive radio: Merits and challenges," *IEEE Wireless Communications*, vol. 16, no. 2, pp. 6–14, 2009.

[20] J. Genachowski, "FCC chairman pushes policy agenda," January 8, 2010. Link: http://ces.cnet.com/8301-31045_1-10430991-269.html (visited 14 June, 2010).

[21] FCC, "In the matter of unlicensed operation in the tv broadcast bands," 2008.

[22] V. Namias, "The fractional order Fourier-transform and its application to quantum-mechanics," *Journal of the Institute of Mathematics and Its Applications*, vol. 25, no. 3, pp. 241–265, 1980.

[23] L. B. Almeida, "The fractional Fourier-transform and time-frequency representations," *IEEE Transactions on Signal Processing*, vol. 42, no. 11, pp. 3084–3091, 1994.

[24] B. Sklar, *Digital communications : fundamentals and applications*. Upper Saddle River, N.J.: Prentice Hall PTR: London, 2nd ed., 2001.

[25] W. Zhiqiang, Q. Daiming, J. Tao, and H. Yejun, "Spectral sculpting for OFDM based opportunistic spectrum access by extended active interference cancellation," in *IEEE Global Telecommunications Conference, 2008.*, pp. 1–5, 2008.

[26] S. Brandes, I. Cosovic, and M. Schnell, "Reduction of out-of-band radiation in OFDM systems by insertion of cancellation carriers," *IEEE Communications Letters*, vol. 10, no. 6, pp. 420–422, 2006.

[27] I. Cosovic, S. Brandes, and M. Schnell, "Subcarrier weighting: A method for sidelobe suppression in OFDM systems," *IEEE Communications Letters*, vol. 10, no. 6, pp. 444–446, 2006.

[28] I. Cosovic, S. Brandes, and M. Schnell, "Method for spectral side lobe suppression in OFDM-based communication systems," 2010.

[29] I. Cosovic and T. Mazzoni, "Suppression of sidelobes in OFDM systems by multiple-choice sequences," *European Transactions on Telecommunications*, vol. 17, no. 6, pp. 623–630, 2006.

[30] S. Pagadarai, R. Rajbanshi, A. M. Wyglinski, and G. J. Minden, "Sidelobe suppression for OFDM-based cognitive radios using constellation expansion," in *IEEE Wireless Communications and Networking Conference, 2008.*, pp. 888–893, 2008.

[31] P. P. Vaidyanathan, "Multirate digital-filters, filter banks, polyphase networks, and applications - a tutorial," *Proceedings of the IEEE*, vol. 78, no. 1, pp. 56–93, 1990.

[32] Q. Zhang, A. Kokkeler, and G. Smit, "An oversampled filter bank multicarrier system for cognitive radio," in *IEEE PIMRC 2008. Personal, Indoor and Mobile Radio Communications, 2008.*, pp. 1–5, 2008.

[33] P. Siohan, C. Siclet, and N. Lacaille, "Analysis and design of OFDM/OQAM systems based on filterbank theory," *IEEE Transactions on Signal Processing*, vol. 50, no. 5, pp. 1170–1183, 2002.

[34] F. D. Beaulieu and B. Champagne, "Design of prototype filters for perfect reconstruction DFT filter bank transceivers," *Signal Processing*, vol. 89, no. 1, pp. 87–98, 2009.

[35] G. Folland and A. Sitaram, "The uncertainty principle: A mathematical survey," *Journal of Fourier Analysis and Applications*, vol. 3, no. 3, pp. 207–238, 1997.

[36] W. Hilberg and P. G. Rothe, "General uncertainty relation for real signals in communication theory," *Information and Control*, vol. 18, no. 2, pp. 103–125, 1971.

[37] M. Abramowitz and I. A. Stegun, *Handbook of Mathematical Functions with Formulas, Graphs, and Mathematical Tables*. John Wiley and Sons, 1972.

[38] E. T. Whittaker, "On the functions associated with the parabolic cylinder in harmonic analysis," *Proc. Lond. Math. Soc.*, vol. 35, pp. 417–427, 1903.

[39] E. Borchi and G. Pelosi, "A quantum mechanical derivation of the general uncertainty relation for real signals in communication theory," *Signal Processing*, vol. 2, no. 3, pp. 289–292, 1980.

[40] G. H. Hardy, "A theorem concerning Fourier transforms," *J. London Math. Soc.*, vol. s1-8, no. 3, pp. 227–231, 1933.

[41] A. Bonami, B. Demange, and P. Jaming, "Hermite functions and uncertainty principles for the Fourier and the windowed Fourier transforms," *Revista Matematica Iberoamericana*, vol. 19, no. 1, pp. 23–55, 2003.

[42] T. S. Chihara, *An introduction to orthogonal polynomials*. New York ; London: Gordon and Breach, 1978.

[43] O. Rosas-Ortiz, "On the Dirac-Infeld-Plebanski delta function," in *Topics in Mathematical Physics General Relativity and Cosmology in Honor of Jerzy Plebanski*, Mexico City: World Scientific Publishing Company, 2002.

[44] V. R. Korostyshevskiy and T. Wanner, "A Hermite spectral method for the computation of homoclinic orbits and associated functionals," *Journal of Computational and Applied Mathematics*, vol. 206, no. 2, pp. 986–1006, 2007.

[45] B. v. d. Pol and H. Bremmer, *Operational calculus : based on the two-sided Laplace integral*. New York, N.Y.: Chelsea Pub. Co., 3rd ed., 1987.

[46] J. L. Rodgers, W. A. Nicewander, and L. Toothaker, "Linearly independent, orthogonal, and uncorrelated variables," *American Statistician*, vol. 38, no. 2, pp. 133–134, 1984.

[47] C. Carrie and J. Webb, "Hierarchal triangular edge elements using orthogonal polynomials," in *Antennas and Propagation Society International Symposium, 1997. IEEE., 1997 Digest*, vol. 2, pp. 1310–1313, 1997.

[48] W. Kozek and A. F. Molisch, "Nonorthogonal pulseshapes for multicarrier communications in doubly dispersive channels," *IEEE Journal on Selected Areas in Communications*, vol. 16, no. 8, pp. 1579–1589, 1998.

[49] B. Razavi, *RF microelectronics*. Upper Saddle River, N.J.: Prentice Hall PTR ; London : Prentice-Hall International, 1998.

[50] M. Tribus and E. C. Mcirvine, "Energy and information," *Scientific American*, vol. 225, no. 3, pp. 179–184, 1971.

[51] Q. Liu and D. A. Pierce, "A note on Gauss-Hermite quadrature," *Biometrika*, vol. 81, no. 3, pp. 624–629, 1994.

[52] G. Leibon, D. N. Rockmore, W. Park, R. Taintor, and G. S. Chirikjian, "A fast Hermite transform," *Theoretical Computer Science*, vol. 409, no. 2, pp. 211–228, 2008.

[53] R. Haas and J.-C. Belfiore, "Multiple carrier transmission with time-frequency well-localized impulses," in *IEEE Symposium on Comm. and Veh. Technology*, pp. 187–193, 1994.

[54] W. Chongburee, *Digital Transmission by Hermite N-dimensional Antipodal Scheme*. PhD thesis, Virginia Polytechnic Institute and State University, 2004.

[55] M. Ghavami, L. B. Michael, S. Haruyama, and R. Kohno, "A novel UWB pulse shape modulation system," *Wireless Personal Communications*, vol. 23, no. 1, pp. 105–120, 2002.

[56] J. A. N. da Silva and M. L. R. de Campos, "Spectrally efficient UWB pulse shaping with application in orthogonal psm," *IEEE Transactions on Communications*, vol. 55, no. 2, pp. 313–322, 2007.

[57] X.-l. Wu, X. Qiu, X.-y. Ning, and D. Lin, "Orthogonal Hermite functions based orthogonal pulse shaping method," in *Electrical and Computer Engineering, 2009. CCECE '09. Canadian Conference on*, pp. 496–499, 2009.

[58] ANSI/IEEE 802.11, "Wireless LAN medium access control (MAC) and physical layer (PHY) specifications," 1999.

[59] ANSI/IEEE 802.11a, "Wireless LAN medium access control (MAC) and physical layer (PHY) specifications - high-speed physical layer in the 5GHz band," 1999.

[60] ANSI/IEEE 802.11g, "Wireless LAN medium access control (MAC) and physical layer (PHY) specifications - amendment 4: Further higher data rate extension in the 2.4 GHz band," 2003.

[61] J. G. Proakis, *Digital communications*. McGraw-Hill series in electrical and computer engineering, Boston: McGraw-Hill, 4th ed., 2000.

[62] T. Weiss, J. Hillenbrand, A. Krohn, and F. K. Jondral, "Mutual interference in OFDM-based spectrum pooling systems," in *IEEE Vehicular Technology Conference, 2004.*, vol. 4, pp. 1873–1877 Vol.4, 2004.

[63] B. Farhang-Boroujeny and R. Kempter, "Multicarrier communication techniques for spectrum sensing and communication in cognitive radios," *IEEE Communications Magazine*, vol. 46, no. 4, p. 80, 2008.

[64] T. Kurt, M. Siala, and A. Yongacoglu, "Multicarrier signal shaping employing hermit functions," in *Proc. EUSIPCO*, 2005.

[65] B. Farhang-Boroujeny and C. H. Yuen, "Cosine modulated and offset QAM filter bank multicarrier techniques: A continuous-time prospect," *Eurasip Journal on Advances in Signal Processing*, 2010.

[66] H. Bolcskei, P. Duhamel, and R. Hleiss, "Design of pulse shaping OFDM/OQAM systems for high data-rate transmission over wireless channels," in *1999 IEEE International Conference on Communications, 1999. ICC99*, vol. 1, 1999.

[67] J. Nielsen, *Niels Bohr Collected Works. Vol. 3. The Correspondence Principle (1918–1923)*. Amsterdam, 1976.

[68] T. Strohmer and S. Beaver, "Optimal OFDM design for time-frequency dispersive channels," *IEEE Transactions on Communications*, vol. 51, no. 7, pp. 1111–1122, 2003.

[69] F. Q. Xiong, "M-ary amplitude shift keying OFDM system," *IEEE Transactions on Communications*, vol. 51, no. 10, pp. 1638–1642, 2003.

[70] B. Sklar, "Rayleigh fading channels in mobile digital communication systems .1. characterization," *IEEE Communications Magazine*, vol. 35, no. 9, pp. 136–146, 1997.

[71] G. S. Prabhu and P. M. Shankar, "Simulation of flat fading using MATLAB for classroom instruction," *IEEE Transactions on Education*, vol. 45, no. 1, pp. 19–25, 2002.

[72] M. Simon and M. Alouini, *Digital communication over fading channels*. Institute of Electrical and Electronics Engineers (IEEE), 2005.

[73] H. Ochiai and H. Imai, "On the distribution of the peak-to-average power ratio in OFDM signals," *IEEE Transactions on Communications*, vol. 49, no. 2, pp. 282–289, 2001.

[74] S. H. Han and J. H. Lee, "An overview of peak-to-average power ratio reduction techniques for multicarrier transmission," *IEEE Wireless Communications*, vol. 12, no. 2, pp. 56–65, 2005.

[75] T. Jiang and Y. Wu, "An overview: Peak-to-average power ratio reduction techniques for OFDM signals," *IEEE Transactions on Broadcasting*, vol. 54, no. 2, pp. 257–268, 2008.

[76] M. Martone, "A multicarrier system based on the fractional Fourier transform for time-frequency-selective channels," *IEEE Transactions on Communications*, vol. 49, no. 6, pp. 1011–1020, 2001.